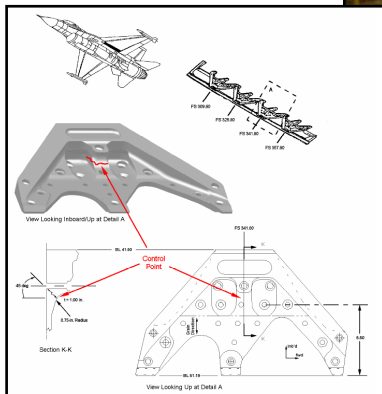


# A REVIEW OF AERONAUTICAL FATIGUE INVESTIGATIONS IN ISRAEL

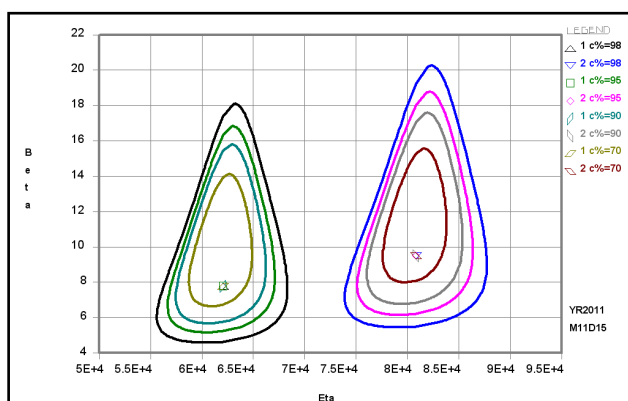
(April 2011 – March 2013)



**Compiled by:**  
**Abraham Brot and Dr. Yuval Freed**  
*Engineering Division*  
*Israel Aerospace Industries*  
*Ben-Gurion Airport, Israel*



*abrot@iai.co.il, yfreed@iai.co.il*



**Presented at the 33<sup>rd</sup> Conference of the International Committee on Aeronautical Fatigue and Structural Integrity (ICAF)**  
**Jerusalem, Israel**  
**4 June 2013**



# **A REVIEW OF AERONAUTICAL FATIGUE INVESTIGATIONS IN ISRAEL**

**APRIL 2011 – MARCH 2013**

## **SUMMARY**

This review summarizes fatigue, structural-integrity and fracture-mechanics investigations that were performed in Israel during the period April 2011 to March 2013. The review includes contributions from Israel Aerospace Industries Ltd. (IAI), Israel Air Force (IAF), Tel-Aviv University (TAU), Ben-Gurion University (BGU), Technion and Rafael.

**Presented at the 33<sup>rd</sup> ICAF Conference  
Jerusalem, Israel  
4 June 2013**



## TABLE OF CONTENTS

	Page
1 INTRODUCTION .....	4
2 FATIGUE ANALYSIS, TESTING AND LIFE EXTENSION .....	4
3 STRUCTURAL INTEGRITY OF COMPOSITE MATERIALS .....	17
4 PROBABILISTIC STUDIES .....	22
5 MISCELLANEOUS .....	23
6 REFERENCES .....	32



# A REVIEW OF AERONAUTICAL FATIGUE INVESTIGATIONS IN ISRAEL APRIL 2011 – MARCH 2013

## 1. INTRODUCTION

The Israel National Review summarizes work performed in the field of aeronautical fatigue in Israel during the period April 2011 to March 2013. The previous National Review [1] covered aeronautical fatigue activities up to March 2011. The following organizations contributed to this review:

Israel Aerospace Industries Ltd. (IAI)  
Israel Air Force (IAF)  
Tel-Aviv University (TAU)  
Ben-Gurion University (BGU)  
Technion  
Rafael

The National Review was compiled by Abraham Brot ([abrot@iai.co.il](mailto:abrot@iai.co.il)) and Dr. Yuval Freed ([yfreed@iai.co.il](mailto:yfreed@iai.co.il))

## 2. FATIGUE ANALYSIS, TESTING AND LIFE EXTENSION

### 2.1 The Strip-Yield Model, Trends in the Prediction of Fatigue Crack Growth Retardation Effects for Aircraft Loading Spectra (C. Matias, E. Katsav, IAI)

The study follows investigations done by A. Brot and C. Matias [2], and presents up-to-date crack growth prediction results of the “Strip-Yield” (NASA) load interaction model that is included in NASGRO 7.0 version Software. It presents that, for typical wing loading spectra, dramatic improvements had been achieved in the NASGRO Strip-Yield Model during the past 10 years. For other typical aircraft loading spectra examined, no significant prediction improvements are being shown.

The evaluation of analytical model included comparisons of predicted results to testing results. The testing data include four airframe industry widely used aluminum alloys. The specimens were tested under four distinct aircraft loading spectra types: Lateral gust loading spectrum, Ground loading spectrum, Wing gust and maneuver loading spectrum and Pressurized fuselage gust and maneuver loading spectrum. The coupons were of two crack configurations: Center cracked tension (CCT) coupon, and Open Hole cracked tension coupon.

Figure 1 presents an example for the improvement in crack growth prediction of the Strip Yield Model (NASA) NASGRO Version 7.0 relative to NASGRO Version 4.2, in comparison to test data, for the wing gust and maneuver loading spectrum.

The following trends were observed:

- The extent of retardation generally decreases as the loading spectrum has a higher mean stress-ratio.
- NASGRO version 4.2 Strip-Yield Model, can reasonably predict crack growth for spectra having stress-ratios in the range of -1 to 0, and have a lower degree of accuracy to predict the extent of retardation for spectra having positive stress-ratios. NASGRO version 7.0 Strip-Yield Model, can reasonably predict crack growth for spectra having stress-ratio of -1, and have a lower degree of accuracy to predict the extent of retardation for the other spectra examined of having stress-ratios in the range of 0.0 and up.
- Significant differences were found in predictions for CCT coupons compared to predictions for Open Hole coupons. The CCT coupons seem to give more reliable results.

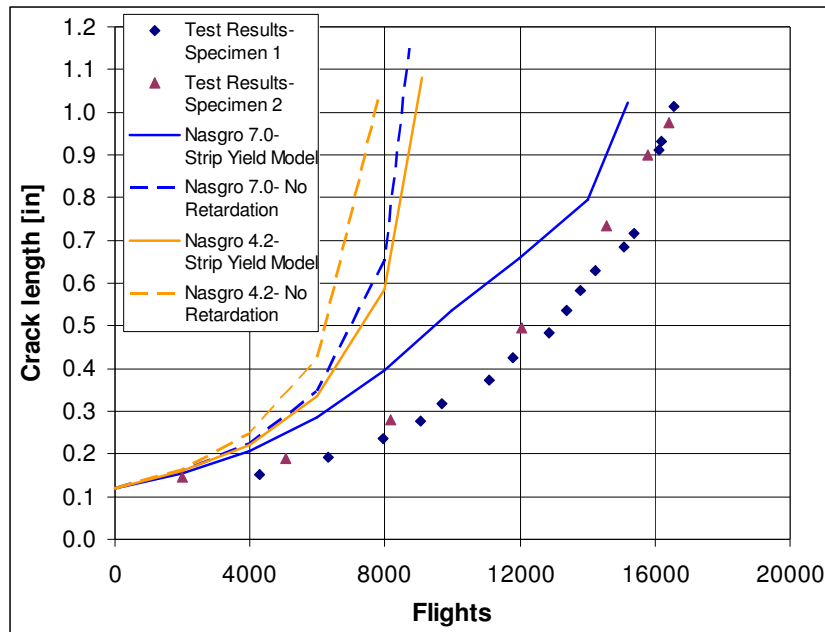


**Figure 1: Comparison of test data to predictions for wing gust and maneuver loading spectrum**

This study will be presented as an oral presentation in the 27<sup>th</sup> ICAF symposium [3].

## 2.2 Developing Strategies to Combat Threats against the Structural Integrity of Aircraft (A. Brot, IAI)

This study traces the evolution of the fatigue life regulations in their aim to counter various threats to the structural integrity of aircraft. The paper begins with the early history of aircraft structural failures and then discusses the current methods for designing and certifying aircraft for adequate fatigue life. Historical structural failures are reviewed and classified into five threat categories:

1. Conceptual failures
2. Unanticipated structural damage
3. Improper repairs or servicing
4. Improper manufacturing and quality-control
5. Aging aircraft (MSD and WFD).

Recent changes to the civil regulations (WFD, FAR-26 and LOV) are then reviewed. The five threat categories are reviewed in light of recent changes to the civil regulations. Fatigue testing, some recent structurally related incidents and the use of composite materials for primary structures are then discussed.

Much of the paper is based on previous research performed by members of the ICAF community, including: Tom Swift, Jaap Schijve, Anders Blom, Robert Eastin, Hans Schmidt, and Jean Rouchon. The above authors were, of course, credited in the paper summarizing this study. The basic aim of the study was using the previous research to trace the evolution of the fatigue life regulations in their aim to counter various threats to the structural integrity of aircraft.

The results of this study were presented at the 52<sup>nd</sup> Israel Annual Conference on Aerospace Sciences, 2012 [4].

## 2.3 Optimizing Inspection Intervals for Aircraft Structures Prone to Multi-Site Damage (A. Brot, IAI)

Damage-Tolerance Analyses (DTA) have been used in civilian aviation for the last 35 years to determine crack inspection requirements, in order to insure the structural integrity of critical structures. Both the FAA and EASA require this analysis for the certification of fatigue critical structures.

Three methods, used to determine the inspection intervals, have been suggested:

1. Classical Method: Based on a damage-tolerance analysis, the number of flights between a "detectable crack" and the "critical crack size" is determined. The inspection interval is selected as 50% or 33% of this value (depending on the criticality of the location).
2. Cumulative Probability of Detection (CPOD) Method: CPOD is the probability that a crack will be detected in any one of the multiple inspections that will be performed throughout the operating lifetime of the aircraft. The acceptable values of CPOD can range from 95% to 99.9%, depending on the criticality of the location. In this manner, the required inspection interval can be selected.
3. Overall Probability of Failure (OPOF) Method: This method accounts for the probabilistic aspects of crack-initiation, crack growth and crack detection throughout the aircraft lifetime, until retirement. The analysis computes the overall expected probability of failure versus the inspection interval. The optimum inspection interval can be calculated from these results.

The *INSIM* (INspection SIMulation) computer program has been developed in order to simulate the entire fatigue environment that a structure must withstand. *INSIM* simulates, in a probabilistic manner, service life variation, service load severity, time to crack-initiation, crack growth history and NDI detection capability.

The damage-tolerance analysis of a typical fuselage lap-splice joint is presented in the paper. This type of structure is prone to Multi-Site Damage (MSD) which can lead to a Widespread Fatigue Damage (WFD) catastrophic failure. The infamous "Aloha Airlines Disaster", which occurred in 1988, was the result of multi-site damage at the fuselage lap-splice joint of the Boeing 737 aircraft.

A typical lap-splice joint is analyzed, and inspection intervals are determined using the three methods described above. From the analyses that were performed, the following conclusions were reached: Determining inspection intervals using the "classical method" results in extremely conservative inspection intervals. This method should only be used when the aim of the analysis is to specify very conservative inspection intervals.

The Cumulative Probability of Detection (CPOD) Method, even when used with a 99.9% CPOD, provides a more realistic inspection interval compared to the classical method.

The Overall Probability of Failure (OPOF) Method (using *INSIM* software) can provide even larger inspection intervals.

Figure 2 shows the overall probability of failure (OPOF) as a function of the HFEC inspection interval and the number of detectable cracks assumed, as obtained from the *INSIM* analysis. The results of this study were presented at the 53rd Israel Annual Conference on Aerospace Sciences, 2013 [5].

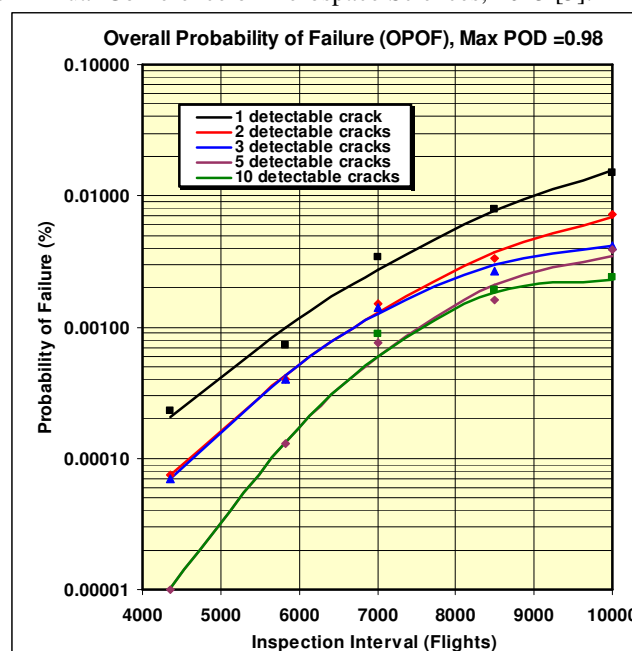


**Figure 2: Overall Probability of Failure (OPOF) as a Function of the HFEC Inspection Interval and the Number of Detectable Cracks Assumed.**

## 2.4 Failure Investigation of Fatigue Cracks Initiated at a Business Jet Vertical Tail Drag Angles (Y. Freed, O. Dolev, IAI)

As part of a damage-tolerance certification program of one of Israel Aerospace Industries business jets, a structurally complete test-article is currently being fatigue tested for two lifetimes (40,000 flights), followed by half a lifetime (10,000 flights) of damage-tolerance testing, with artificial flaws inflicted at critical locations. Residual strength tests, under limit loads and cabin pressurization, will be performed in the presence of large cracks at several critical locations. This will be followed by a selected teardown inspection.

During one of the minor inspections conducted within the full-scale testing, three surface cracks were detected at the radius of two drag angles which attach to the vertical tail and the aft fuselage. The cracks were detected and verified by means of two different NDI methods, namely, High Frequency Eddy Current (HFEC) and liquid penetrant. The drag angle and the liquid penetrant indication are shown in Fig. 3. The main role of the drag angle is to support the structural reaction to the (T-shape) vertical tail yaw rotation during flight, and it is not considered as a principal structural element (that is, its loss will not lead to catastrophic failure of the aircraft). However, it was decided to investigate the root-cause of the crack-initiation and to suggest and implement design changes to improve the product.

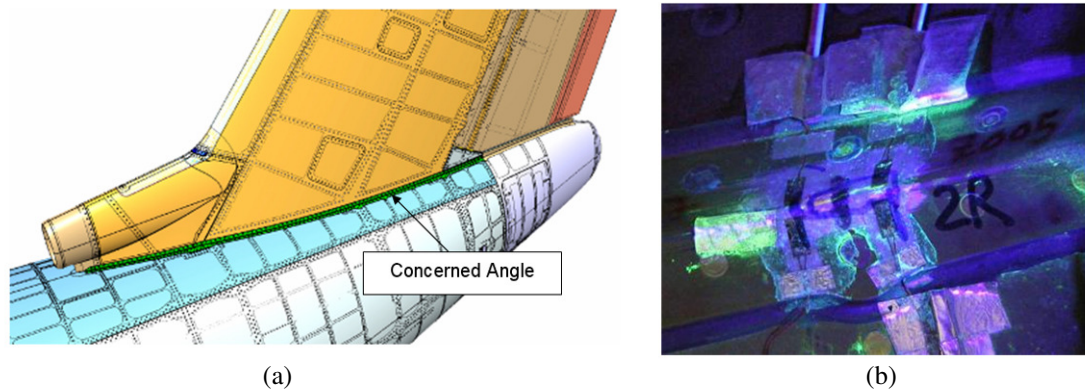


**Figure 3: (a) The drag angles. (b) Liquid penetrant indication of crack at the angle corner radius**

As part of the root-cause analysis, both drag angles were instrumented by means of strain gages to validate the finite-element predictions (see Fig. 4). These measurements were further verified by means of photoelastic stress measurements that also account for strain and stress distributions rather than the localized strain-gage measurements. It was concluded that the drag angle is too stiff, and therefore, it is participating in carrying the vertical tail bending moment (this was not its original role during the design process). These deflections, occurs several times per flight, led to the nucleation of fatigue cracks.



**Figure 4: An example of strain gage instrumentation of the RHS drag angle**

Several design improvements were suggested, such as material replacement, improved heat treatments, fastener relocation, and disconnecting the aft fuselage frames from the drag angle. The chosen design improvement was implemented in the test article and in fleet, and further measurements conducted showed significant reduction of the strain levels in the drag angle upon tail bending. This reduction is sufficient to ensure the drag angles a free of cracking period which is much longer than the aircraft design service objective.

A paper addressing this investigation was presented at the 53<sup>rd</sup> Israel Annual conference on Aerospace Sciences, 2013 [6].

## 2.5 G280 Executive Jet – Full Scale Fatigue Testing (Y. Freed, IAI)

Israel Aerospace Industries and the Gulfstream Aerospace Corporation have jointly developed the G280 super mid-size executive jet. The aircraft has a range of 3,400 nautical miles at a maximum speed of Mach 0.85. It can cruise at altitudes up to 45,000 feet. The first flight of the G280 took place during December 2009. Certification of the G280 to the FAA, EASA, CAAI and TCCA regulations were completed, and type-certificates were obtained. Deliveries of the G280 began in 2012.

The aircraft is powered by twin Honeywell HTF7250G engines, each producing 7,445 pounds of thrust. The G280 is capable of nonstop flight from New York to London or from London to Dubai. The aircraft has a very roomy and quiet cabin. The cabin environment includes 100% fresh air and a cabin altitude not exceeding 7,000 feet. The Design Life Goal (DLG) of the G280 is 20,000 flights or 36,000 flight-hours.

As part of its damage-tolerance certification program, a structurally complete G280 test-article is currently fatigue tested for two lifetimes (40,000 flights) followed by, approximately, half a lifetime (10,000 flights) of damage-tolerance testing, with artificial flaws inflicted at critical locations. Residual strength tests, under limit loads and cabin pressurization, will be performed in the presence of large cracks at several critical locations. This will be followed by a selected teardown inspection.

The test article consists of a structurally complete airframe, including the entire empennage structure. The vertical stabilizer, horizontal stabilizer, elevators, scissors, pivot fitting and dummy horizontal stabilizer trim actuator (HSTA) are included in the fatigue test-article. Figure 5 below shows the G280 fatigue test-article mounted in its loading fixture. Figure 6 shows a schematic view of the fatigue test setup, and showing the loading system.



**Figure 5: Complete G280 Airframe Mounted in its Fixture and Ready for Fatigue Testing**

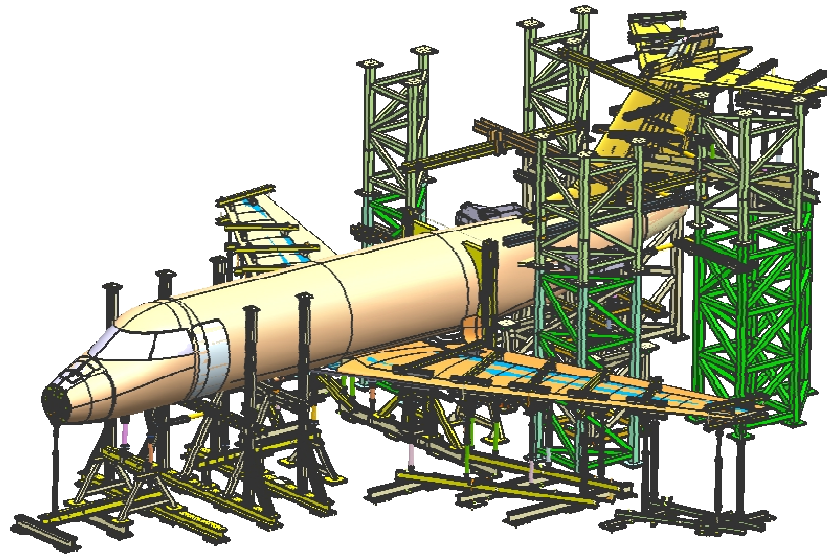


**Figure 6: Schematic View of the G280 Fatigue Test Setup**

The full-scale fatigue test spectrum includes a complete set of symmetric and asymmetric fatigue loads, including engine thrust reverser buffeting loading on the empennage and a suitable representation of engine support loading and main landing gear backup structure loading. The loading spectrum contains 57 cycles per flight (approximately 10-12 minutes per flight). Loads are applied through 58 loading zones and are reacted at six locations. A cabin pressure differential of 9.2 psi is applied during each flight. Periodic inspections for cracks are performed at suitable intervals using various NDI methods. Periodically, a total of more than 1500 strain-gage measurements are recorded, under a set of calibration loads, in order to determine if any significant fatigue damage has occurred at various critical locations. To date, the test has completed 25,000 flight cycles.

At the end of two lifetimes (40,000 flights) of cyclic testing, artificial flaws will be introduced at several critical locations. The damage-tolerance test phase will be continued for another half a lifetime (10,000 flights), in order to ensure that sufficient crack growth data will be obtained. In addition to the artificial flaws, certain cracks detected during fatigue testing will not be repaired and their crack growth rates will be closely monitored during the damage-tolerance testing. Crack growth gages will be installed at crack tips to monitor the growing cracks until the end of the damage-tolerance phase of this test.

At the end of the cycling tests, a number of residual strength tests will be performed, including a two-bay crack in the fuselage. Some of the existing cracks will be enlarged significantly before the application of the residual strength loads. After the series of residual strength tests, two cases of ultimate load will be applied to the composite material horizontal stabilizer.

At the end of the fatigue test, a selected teardown inspection will be performed, where selected areas of the test-article will be disassembled and inspected for cracks.

To date, after 25,000 simulated flights, several cracks were detected in the test-article. All of these cracks were addressed, and relevant design improvements and retrofits were employed in fleet to ensure the structural integrity of the aircraft.

The current activity reported here is a continuation of an activity that was reported in the 2009 and 2011 Israel National Review. It should be noted that the name of the aircraft was changed from G250 to G280 for marketing reasons.

A detailed summary of this test was presented at the 52<sup>nd</sup> Israel Annual conference on Aerospace Sciences, 2012 [7].

## **2.6 G280 Executive Jet, Rudder Fatigue Test (E. Eigenberg, IAI)**

This activity is a continuation of an activity that was reported in the 2011 Israel National Review [1].

A fatigue test for the rudder assembly was performed in order to verify the structural adequacy of the RTM manufacturing procedure, including a "one-shot" manufacturing of the rudder torsion box. Initial flaws and

BVID, demonstrating typical manufacturing flaws, were included in the test article in its critical locations. Fig. 7 shows the rudder assembly test-article mounted in its test fixture.

The first stage of testing consisted of two lifetimes (40,000 flights) of spectrum loading. The spectrum loading included load enhancement and environmental factors, to account for material scatter and environmental effects. The two lifetime spectrum loading was followed by loading the rudder to its ultimate load.



**Figure 7: The G280 Rudder in its Test Fixture**

After completion of ultimate loading, severe damages were inserted to the rudder structure. Several of these damages were repaired, and the remaining damages were left as is. An example of these CVID damages is shown in Fig. 8. In the presence of these damages the test-article was loaded again at spectrum loading for an additional half lifetime. These damages were closely monitored during cycling. No growth was detected during scheduled NDT inspections. At the end of the damage tolerance phase, a residual strength test was conducted to validate the structural integrity of the rudder.



**Figure 8: Typical CVID damages**

## 2.7 Several Models for Crack Propagation Process (G. Maymon, RAFAEL)

In this research, the effect of the R-ratio on the crack growth prediction is intensively investigated. Four major models for crack propagation process are reviewed: The “classical” Paris-Erdogan linear model (that does not account for the effect of R-ratio), the NASGRO computation code model, the Forman equations and the “unified” approach. The latter is evaluated in more detail, as it is less known to the fracture mechanics community.

The “unified” approach is described in many papers by Sadananda and Vasudevan [8-10]. According to these studies, the growth of the crack depends on both  $\Delta K$  and  $K_{max}$  (which is a function of the R-ratio), and in order for a crack to grow, two thresholds values must be met. According to this approach, the local driving force of cracks is comprised of two stresses – one originated from the far field stress-intensity factor and one from local

internal stresses close to the crack tip. These local stresses “create” local R values near the crack tip, which are different from the far field R value. The internal stresses were measured [9] and compared to finite-element computations. By using this approach, the behavior of both short cracks and long cracks can be treated using one “unified” growth law. This approach is supported by data analysis of many previous experimental results for many different materials described by numerous authors and laboratories.

An example of the two threshold values is shown in Fig. 9 below. The results of this study were presented at the 53<sup>rd</sup> Israel Annual conference on Aerospace Sciences, 2013 [11].

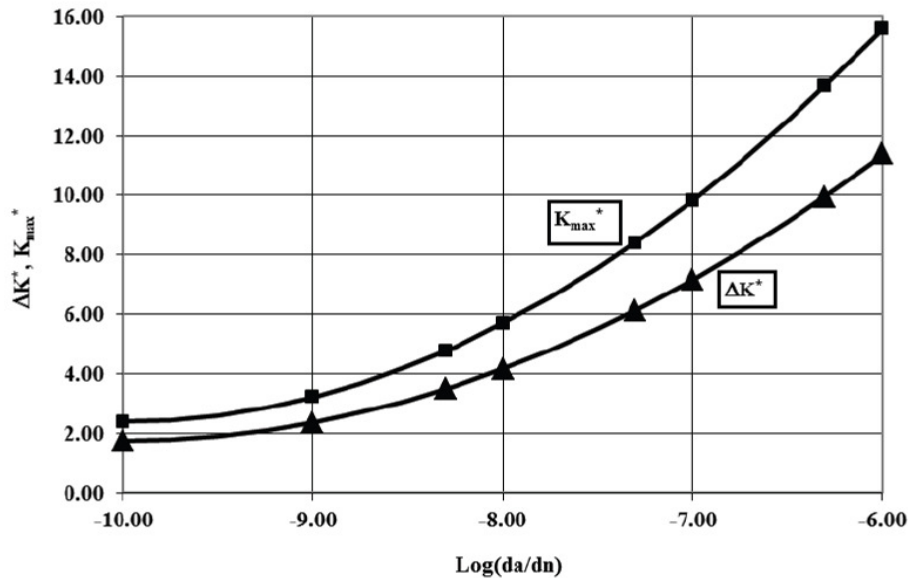


**Figure 9. Threshold values as a Function of da/dN**

### 2.8 Severity Factor Evaluation of the IAF Block 10 F-16 Aircraft (K. Levi, T. Knitel, N. Shemesh, M. Ben-Noon, IAF)

The limit of validity (LOV) of the F-16 pre-block 40 aircraft was based on several activities: full scale durability test (FSDT), component test and analyses. The outcome of these activities enabled to determine the LOV to be limited to 10,800 flight-hours. The LOV flight-hours are given in terms of the design equivalent flight-hours (DEFH) which reflect the baseline spectrum that was used in the tests and analyses.

Since the aircraft do not necessarily operate in the same manner as was considered in the design stage, some of the airplanes experience moderate usage while most of them experience relatively severe usage spectrum with respect to the baseline. As part of IAF service life evaluation program, it was needed to determine the age of each individual pre-block 40 aircraft with respect to the LOV.

Since the IAF block 30 aircraft have flight recording system and an IAT capability, it is easier to evaluate the age of the aircraft in terms of DEFH. The Israeli block 30 aircraft have accumulated about 3,500 actual flight-hours (AFH), however the Israeli usage severity with respect to the design spectrum has been found to be higher by 1.85. In other words, IAF fleet has accumulated on average about 6,500 DEFH. In Fig. 10, the method of evaluating the equivalent flight hours of each aircraft is depicted. The IAT output provides the “ending flaw size” for each aircraft and based on the baseline crack growth curve the DEFH is determined. The severity factor (SF) is given by the ratio of the DEFH and AFH.

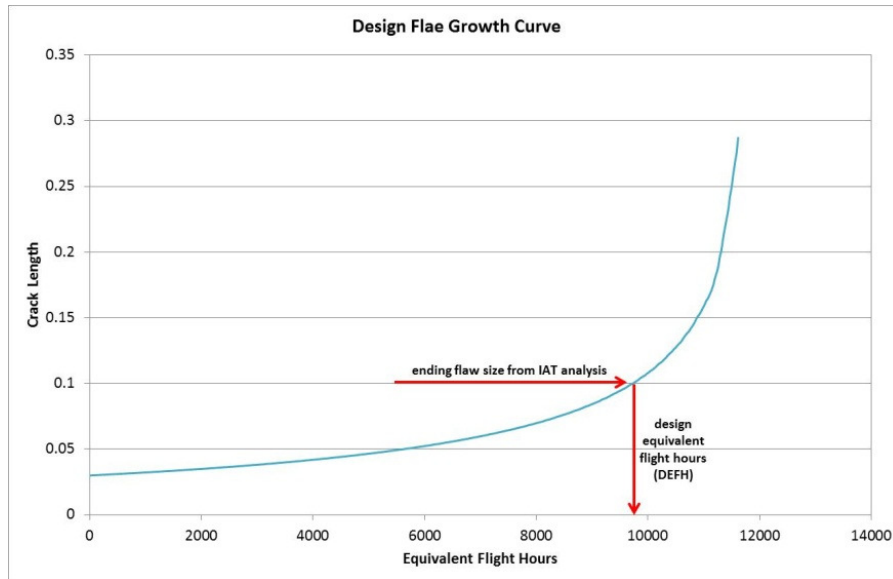


**Figure 10: Evaluation of design equivalent flight hours (DEFH)**

In Figure 11 the SF distribution of the IAF block 30 fleet is depicted. It can be seen that based on extreme value PDF function fitting the expectancy (E) is 1.91 and the standard deviation ( $\sigma$ ) is 0.143.

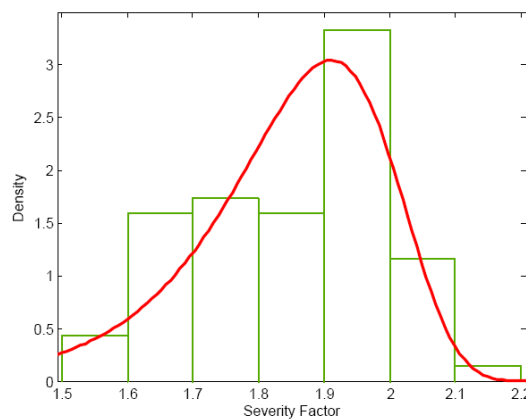
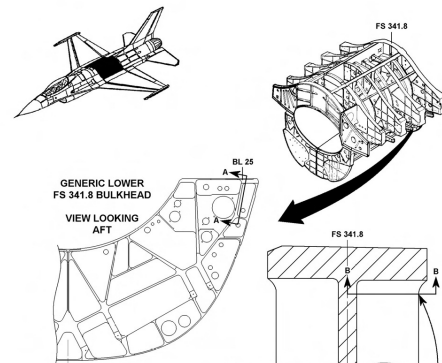
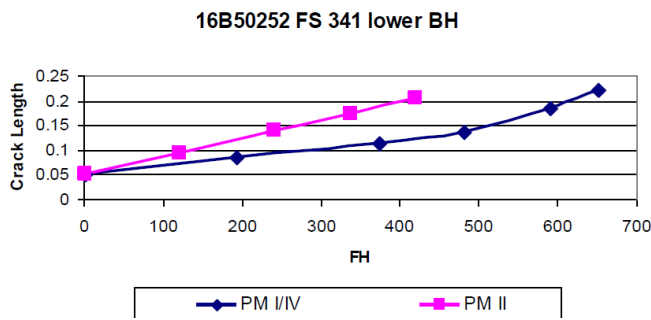


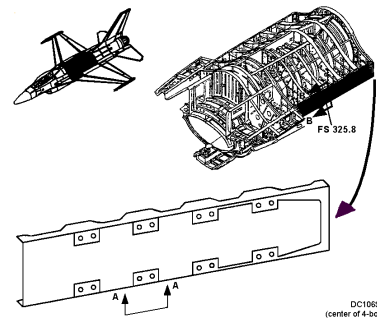
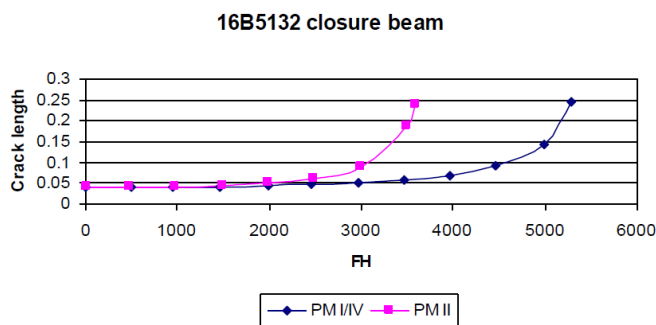
**Figure 11: F-16 block 30 SF fleet distribution**

The IAF block 10 aircraft do not have flight recording system. Hence it is difficult to determine the age of these aircrafts in terms of DEFH. It is important to mention that the IAF block 10 aircraft are aging and may have reached their LOV. For instance, the leader of the fleet aircraft has accumulated about 6,000 flight-hours. Therefore, in order to carry on operating the fleet it is essential to evaluate the SF for each aircraft in the fleet.

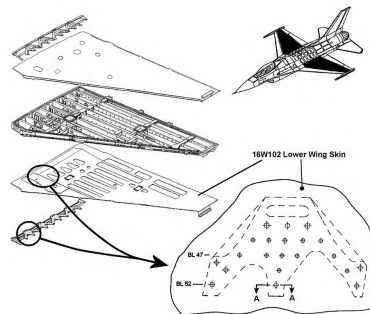
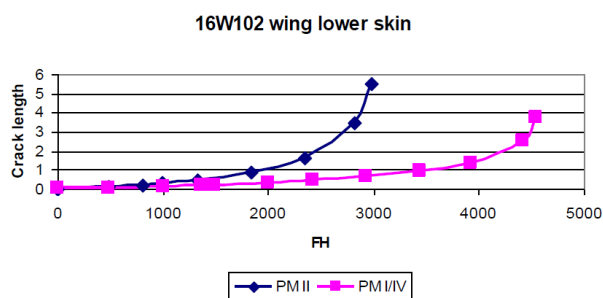
The IAF F-16 block 10 SF was evaluated based on two independent methods. The first one is analytical and the second one is based on actual in-service findings. In the first method, the durability and damage tolerance analysis (DADTA) of block 10 & block 30 were used. Three representative control points in the area of the center fuselage and the root of the wing were selected. Each one of the control points had the same features (geometry, stress gradient, loads, initial crack size and etc.). For each control point the ratio between the block 30 and block 10 lives were calculated and provided their relative SF. It can be seen in Fig. 12 that the severity factor between block 30 and block 10 is approximately 1.51 (1.54, 1.47, and 1.527 for each control point by itself).



(a)



(b)



(c)

**Figure 12: F-16 Control Points that were Chosen for Analytical Evaluation**

The second method is based on comparison between block 10 and block 30 fleet cracking. For this purpose, fleet findings in the wing attach fittings (WAF) which are installed in the area of interest (wings root) were selected for the evaluation (see Fig. 13). In the block 30 aircraft the findings in the WAF inspected after accumulating 2,000 FH on average while in the block 10 aircrafts these cracks detected after 3,000 FH on average. This fact leads to the conclusion that the severity factor between these two models is also 1.5 as it was determined in the first method. A comparison of the fleet finding is depicted in Fig. 14.



The recognition algorithms use up to 5 different parameters to distinguish between the maneuvers. The development process was comprised of 3 stages: (1) characterization of maneuvers using a scarce set of two flight-tests; (2) broadening recognition by manually reviewing recognition results for unmarked squadron flights; (3) verification of the RRA against another (third) flight test that which was performed only after the recognition algorithm was completed. All the maneuvers in this flight were successfully recognized, as shown in Fig. 15.

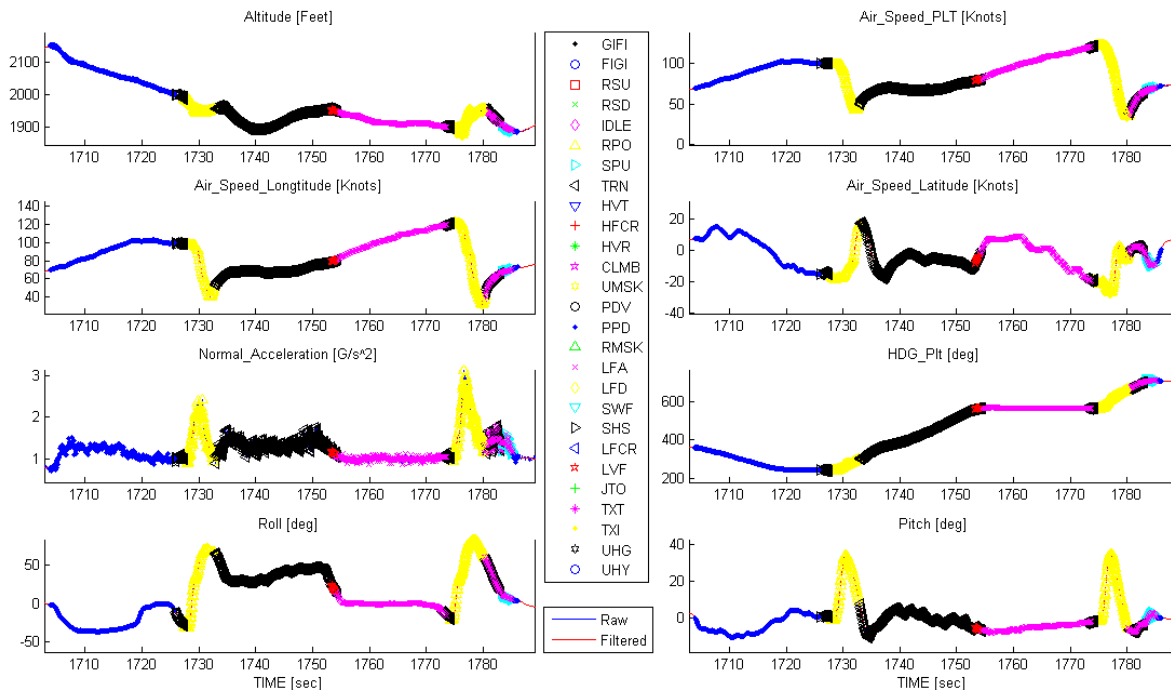


**Figure 15: Recognized Maneuvers in the Verification Flight Test.**

Since RRA based estimations are less conservative than questionnaire-based estimations, components retirement times are expected to change. During the development of the RRA, an initial sensitivity study of the AH-64 Main-Rotor (MR) Collective Actuator Bracket retirement time was examined. The life based on pilot questionnaires resulted in 2644 FH while repeating the calculation based on RRA resulted in 4789 FH. More work on this matter is planned to be performed.

The presented work is still at an early stage of development. Thorough manual verification using unmarked squadron flight will be continually performed, while adding new maneuvers to the recognition algorithms.

This study was presented at the 52<sup>nd</sup> Israel Annual Conference on Aerospace Sciences, 2012 [12].

## 2.10 Emergency Repair Design for a Refueling Boom (S. Kedem, IAF)

The IAF operates Boeing 707 aircraft for aerial refuelling. In March 2011, irregular motions of the boom and its ruddervators were seen. After landing, the boom was inspected and cracking was detected.

According to the IAF investigation, it has been determined that cracks had initiated due to fatigue in the inner housing. In order to maintain high operational availability of the aerial refuelling capability, an emergency composite repair was designed, complying with two requirements:

1. The repair must be applied as quickly as possible at the operational level.
2. In order to suppress development of fatigue cracks, the repair must strengthen the inner housing and relieve some of the stresses from the cracked region.

The structure of the boom is rather complicated, thus a conventional repair may not comply with the aforementioned requirements, mainly due to the time it would take to disassemble, repair and reassemble. In

order to meet the requirements, a unique repair concept was adopted, so only the intact outer structure is reinforced, while leaving the inner cracked structure as is. Figure 16 shows the implementation of the repair.

A comparative analysis was performed – comparing the stresses and strains in the inner housing between a repaired and a non-repaired boom. The FEM analysis showed a reduction in stresses and strains following the application of the repair.

In order to verify the analysis, a ground test was performed. The experiment has confirmed the validity of the finite element analysis. Test results showed a reduction of approximately 18% in equivalent stresses underneath the repair. Figure 17 shows the application of strain-gages.

It has been validated that the composite repair does relieve stresses from the inner housing and retards rapid propagation of fatigue cracks. Both analysis and ground test showed a reduction of stresses and strains in the inner tube after applying the repair on the boom. The repair concept was proven to be efficient in retarding crack propagation in the inner tube by reducing its stress and strain levels.

This study will be presented at the 27<sup>th</sup> ICAF Symposium, 2013 [13].



**Figure 16: Implementation of the Repair**

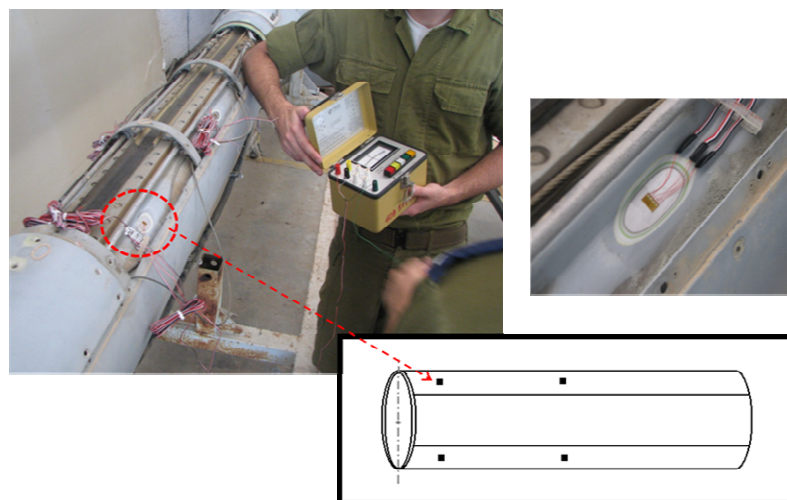


**Figure 17: Applying Strain-Gages on the Boom**

### **2.11 Helicopter Swash-Plate Ball Bearing Modeling For Faults Simulation (G. Kogan, J. Bortman, BGU)**

The main role of a health usage monitoring system (HUMS) in aviation is to improve safety-of-flight by preventing unpredictable mechanical failure of critical components. Besides safety benefits, HUMS also offers potential economic savings achieved by changing the maintenance policy of certain components from conventional scheduled maintenance procedure to Condition Based Maintenance (CBM). Today HUMS programs are mainly based on ground calibration tests. Such tests take a long time and are costly. It was our goal



to improve the modeling tools which might reduce the time and budget needed to implement the HUMS approach.

The ball bearing is an important part of rotating machinery whose main function is reducing the rotational friction and wear while supporting radial and axial loads. Rotating machinery faults are often caused by bearing failure. A well-established method for detecting local defects in rotating element bearings is vibration analysis. However, the effect that structural defects have on the vibration signature suffers from a dearth of research. The main goal of the proposed model, therefore, is to study how anomalies in bearing structure affect bearing behavior.

During this research, a new 3D "global" dynamic ball bearing model was developed. The aim of this generic model is to provide capabilities of simulating the dynamical response of a bearing with a wide spectrum of defects allowing development of condition indicators for diagnostics and prognostics of bearing health status. In addition, a 3D "local" finite element model was build and employed to simulate the local interaction between the bearing components as well as their interaction with the structural anomalies. This process improves the accuracy of the dynamic model.

The dynamic model was validated by comparison to an analytical solution and the known behavior of bearings with a local defect. After the validation, the model was implemented for a structural anomaly case. The presented results, for a nominal case, are the displacement, the acceleration, and the load that is acting on the ball. The model was used to examine the influence of different parameters, such as, operating conditions; bearing geometry and fault characteristics. The simulation results were compared to experimental results and good agreement was shown.

### **3. STRUCTURAL INTEGRITY OF COMPOSITE MATERIALS**

#### **3.1 Accelerated Testing Methodology for the Predictions of Long Term Strength and Durability of Composite Materials in a Marine Environment (Y. Freed, Y. Buimovich, IAI)**

It is well known that the strength and the durability of air vehicles made of composite materials strongly degrade when utilized in marine environment (exposed to varying temperatures and moisture). With the increase use of composite materials as primary structures in light-weight unmanned air vehicles that operates intensively in a marine environment, the ability to predict long term behavior of composite materials becomes essential. Since modern aircraft are designed to operate for 30 – 40 years, it is needed to establish an accelerating testing methodology that can be employed in determination of material design allowables and can even replace long-term testing.

Most of aviation products made of composite materials are certified using AC 20-107B methodology, in which *"the effects of repeated loading and environmental exposure which may result in material degradation should be addressed in the static evaluation..."* and *"Fatigue substantiation should be accomplished by... accounting for the effects of the appropriate environment"*. The common approach to account for the environmental effect is to perform hot-wet coupon tests or, alternatively, reduce the material strength and fatigue allowables (or increasing the applied loads) by a certain level. For instance, MIL-HDBK 17 recommends applying a load enhancement factor of 1.06 as an environmental compensation factor. This is certainly a conservative approach that can be employed when no other relevant engineering data is available.

In this study, an accelerating testing methodology for the determination of residual strength and durability degradation of the composite material upon time is introduced. This method was originally developed to determine non-destructive material properties of polymers, but it can be shown that it may be applicable to certain types of composite materials as well [14]. The basic idea of this method is to perform viscoelastic testing at several elevated temperature and water absorption states to obtain the relation between the temperature, the moisture and the testing time periods. This relation, usually referred to as a **'Time-Temperature-Moisture Superposition Principle' (TTMSP)**, holds for creep, residual strength, and fatigue behavior of the unidirectional composite material, under certain limitations. With additional sets of simple constant strain-rate and fatigue coupon tests, the environmental effect on the mechanical properties of the composite material can be determined. This procedure is schematically described in Fig. 18.

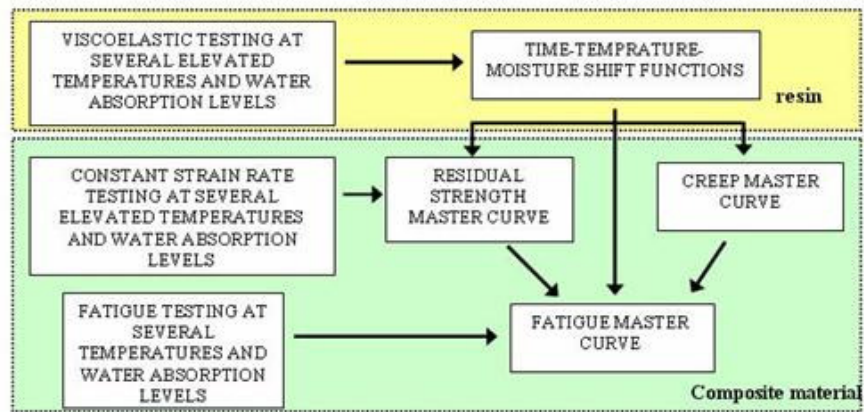


**Figure 18. Schematic Description of the Accelerating Testing Methodology.**

The outcome of this study is a set of master-curves, in which the long term behavior of the composite material is described in terms of applied loads, number of cycles to failure, load frequencies, and operational temperatures and moisture levels. Both three point bending and tensile specimens are tested.

The results will be presented as an oral presentation in the 27<sup>th</sup> ICAF symposium, 2013 [15], which will include the test results and the conclusions drawn from them. These are compared to a previous study, presented in the 26<sup>th</sup> ICAF symposium, 2011 [16], in which the T300/913 unidirectional composite material was analyzed by means of the same accelerated testing approach but at dry conditions. An example of typical master curve is shown in Fig. 19 [15].

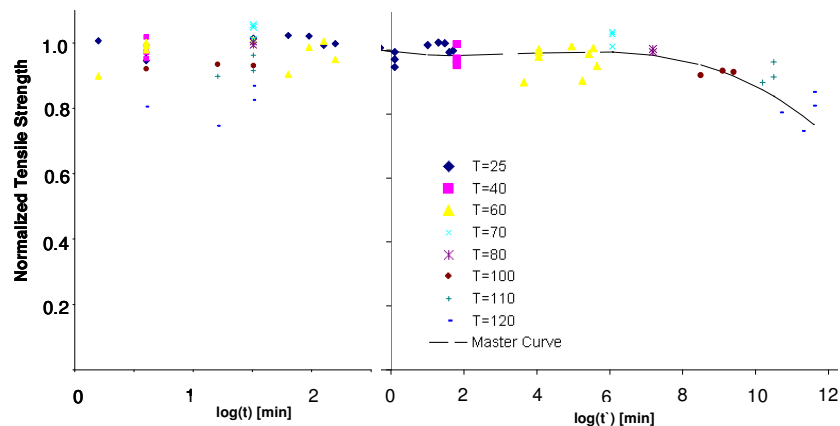


**Figure 19. Tensile Residual Strength Master-Curve in a Moist Environment.**

### 3.2 Fiber-Optic Based Technology for UAV Structural Health Monitoring (I. Kressel, IAI; M. Tur, TAU)

This activity is a continuation of work reported in the Israel National Review of 2011 [1].

In recent years the Unmanned Air Vehicle (UAV) industry moved towards applying the commercial manned aircraft structural airworthy regulations (STANAG 4671). According to these directives, the increasing use of advanced composite materials for UAV structural components requires special attention. Extensive use of bonded, integral structural concepts for main components, including the wing and fuselage, imposes a great challenge since a bond line with mechanical properties lower than expected, mainly due to a poor chemical bonding, is undetectable by conventional NDT methods. In addition, conventional periodic inspection methods of such critical structural components are hindered by limited accessibility and require highly trained and costly technicians. Special care must also be given to inspection methodologies used since UAVs are often operated at remote sites where technical resources are limited.

The recently introduced Structural Health Monitoring (SHM) concept is aimed towards real-time structural assessment of the individual air vehicle, alerting for maintenance action only upon need. One of the ways of implementing an online SHM system is by using fiber optic sensing technology. The most attractive capability of fiber optic sensing technology is the possibility of sensor multiplexing. By utilizing this ability one fiber can incorporate hundreds of sensors and, therefore, can interrogate a relatively large area.

The key to an effective SHM system for aircraft structures is not only the appropriate sensor selection and measurement, but also the processing of the sensor data to deduce information in terms of operating loads and/or structural damage, if any. This work presents lessons learned in the development of SHM systems, and proposes a further course of action, based on ground and flight testing of an airworthy SHM system for an Unmanned Air Vehicle (UAV).

The Nishant UAV (Fig. 20), designed and manufactured in India by Aeronautical Development Establishment (ADE) was selected as the test-bed for the evaluation of this SHM concept.



**Figure 20: The Nishant UAV on the launcher**

In order to track the boom loading, two fibers were embedded at the centers of the boom ("center Fibers", CH2, CH3 in Fig. 21) and another two Fibers were embedded near the corners ("side Fibers", CH1, CH4 in Fig. 21). Four Fiber Bragg Grating (FBG) sensors were imprinted on each Fiber. Measured readings are shown in Fig. 22 for the duration of the entire flight.

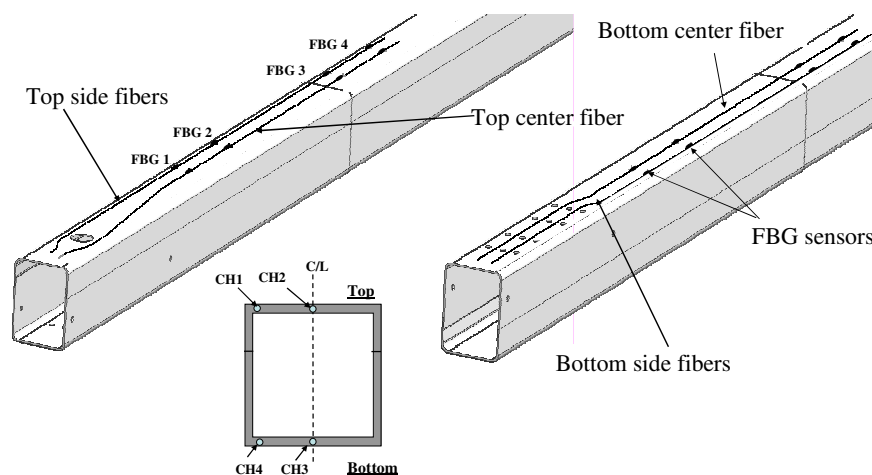


**Figure 21: Boom general layout and routing of the embedded optical fibers inside the boom. 16 FBGs were located at points of interest.**

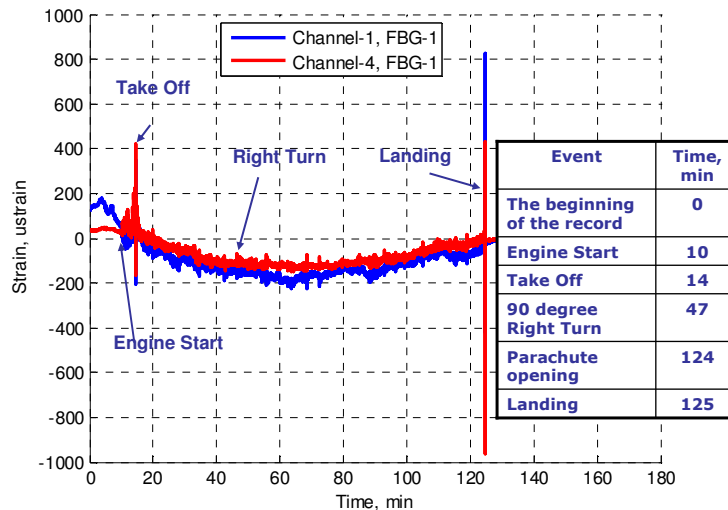


**Figure 22: Typical FBG readings during flight**

Real-time measurements were taken for different flight segments. Furthermore, a load and damage tracking algorithm was constructed, based on the detection of deviations from the expected modal behavior. After employing this algorithm to measurements conducted by the FBG sensors, it was seen that the UAV boom fully recovers from its landing impact and remains intact.

This research was conducted in collaboration with A.C.R Pillai, M.H. Prasad and A. K. Yadav from the Aeronautical Development Establishment in Bangalore, India, and N. Gupta, S. Sathya and R. Sundaram from the National Aerospace Laboratories in Bangalore India

The results of this study will be presented as an oral presentation in the 27<sup>th</sup> ICAF symposium 2013 [17].

### **Health and Usage Monitoring of an Aging Helicopter Tail using Fiber-Bragg Grating Sensor Net (N. Shemesh, IAF; I. Kressel, IAI and M. Tur, TAU)**

This activity is a continuation of a study that was reported in the 2011 Israel National Review [1].

A Fiber-Bragg-Grating (FBG) based advanced health and usage monitoring sensing net, imbedded in a co-cured composite patch repair for aging helicopter structure, is proposed and demonstrated. Vibration loads, patch debonding and crack propagation rate can be monitored using a low spatial resolution of FBG sensor net embedded in a composite patch. During the curing process of the patch, the strain field induced by thermal mismatch between the composite patch and the metal substrate is measured. Since the strain field in the composite patch is affected by both growing crack in the metal substrate and patch-to-substrate debonds, it is possible to identify and track the damage propagation during service by correlating these strain measurements with a numerical model.

The concept of using bonded composite repairs for aging metallic aircraft has been proven to be a preventive measure as well as a method for retarding future growth of existing damage. The main advantages of a bonded repair is its smoother load transfer, absence of additional stress concentration, good fatigue and damage-tolerance behavior of the composite patch and its ease application on curved surfaces. However, one of the disadvantages of bonded composite repairs is the lack of non-destructive means for structural integrity assessment during the application and service of such repairs. Nowadays, most commercial inspection procedures for bonded composite structures are based on detecting voids using ultrasonic techniques at scheduled maintenance intervals. However, in case of a bonded repair on a cracked structure, ultrasonic inspection is ineffective in detecting the crack propagation and may lead to incorrect structural integrity assessment. In such a case, a separate, additional inspection procedure is required for the crack detection.

During the last decade, smart repair concepts were introduced in a number of publications, which aimed toward a real-time repair integrity assessment based on direct monitoring of internal strains, using embedded sensors. This work presents experimental and numerical evaluation of an advanced co-cured smart composite patch repair applied on an IAF helicopter tail, based on an embedded, low spatial resolution, optical FBG sensor net. The

FBG readings combined with numerical predictions are used for direct assessment of repair integrity during service.

The proposed Structure Health Monitoring concept is based on tracing the residual thermal strains using embedded FBG sensors. The principle behind this approach relies on the fact that in-service changes in the induced composite to metal bonding thermal strains can be measured and tracked. Thermal stresses are developed because of the large difference in the thermal expansion coefficients between the patch composite materials and the metallic substrate. For a 120°C cured patch, at room temperature, this mismatch induces compression stresses in the patch and tension in the metallic structure. Some researchers have shown that a crack in a metallic structure, repaired by a bonded composite patch, will propagate at a much lower rate compared to an unrepaired one. However, patch debonding deteriorates the efficiency of retarding the crack propagation and may lead to further growth of the original debond. Consequently, when the crack grows, the thermal induced strain field in the patch, at the vicinity of the crack, is reduced and enables to detect the crack propagation with and without the patch debonding.

Based on these guidelines, a health monitoring system, which consists of bonded patch with imbedded FBG sensors, was attached to an aging helicopter tail, as shown in Fig. 23. Crack tracking currently performed periodically. Linear dependency of FBG readings with respect to temperature is observed (Fig. 24). This implies no change in repair integrity over 550 Flight Hrs.

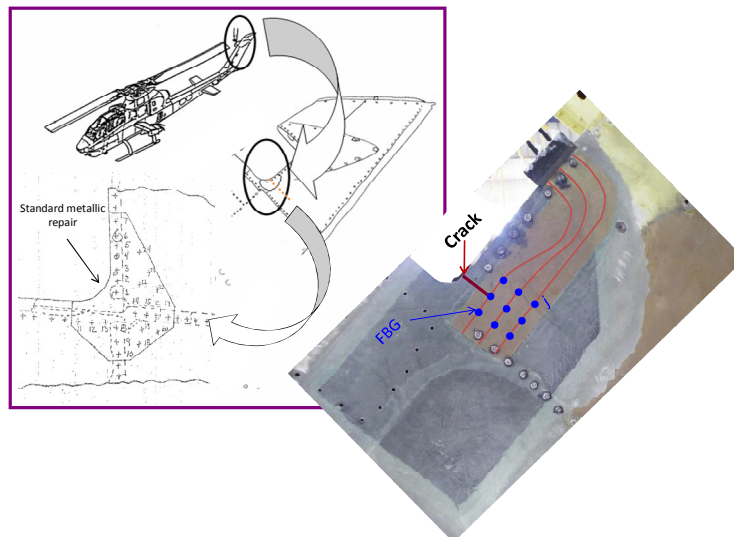


**Figure 23: Repair patch that includes FBG sensors attached to the helicopter tail.**

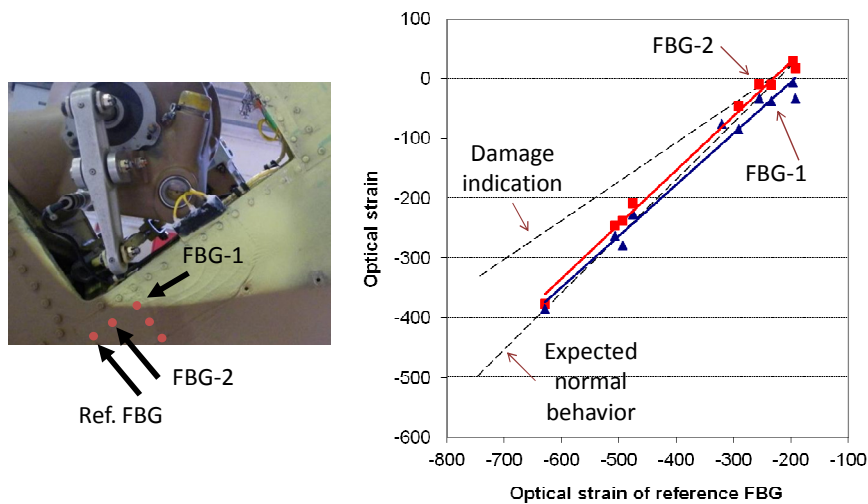


**Figure 24: FBG measurements during test.**

## 4. PROBABILISTIC STUDIES

### 4.1 Substantiating Fatigue Lives of Structures by Using a Weibayes Distribution, (A. Brot, IAI)

This topic was first presented in the Israel National Review in 2011 [1]. The following is a continuation of this study.

The Weibull statistical distribution generally has two unknown parameters, the "characteristic life" ( $\eta$ ) and the "shape-factor" ( $\beta$ ). Often, it is assumed that the shape-factor is a known parameter, for example, as a function of the specific material or alloy. Many experimental investigations have been performed that show that  $\beta \cong 4$  for aluminum structures and  $\beta \cong 3$  for titanium and moderate strength steel. It should be noted that a large value of the shape-factor corresponds to little scatter of results, while a small value implies much scatter.

When a Weibull analysis is performed under the assumption that the shape-factor is *a priori* known, this is sometimes called a "**Weibayes Analysis**". A more precise name for this procedure is a one-parameter *Weibull analysis (using an assumed shape-factor)*. Making this assumption greatly simplifies the analysis, but the assumption of a known shape-factor must be verified by testing or be taken from valid "historical failure data". In a Weibayes analysis, where the shape-factor ( $\beta$ ) is assumed to be known, the characteristic life ( $\eta$ ) can be easily determined from a series of fatigue tests.

A fatigue test was performed on ten nearly identical coupons. The purpose of this test was to establish the representative Weibayes shape-factor that will be used in the structural reliability analysis of 7050-T74 aluminum structures.

Figure 25 is a description of the 7050-T74 aluminum coupon that was tested, all dimensions are in mm.

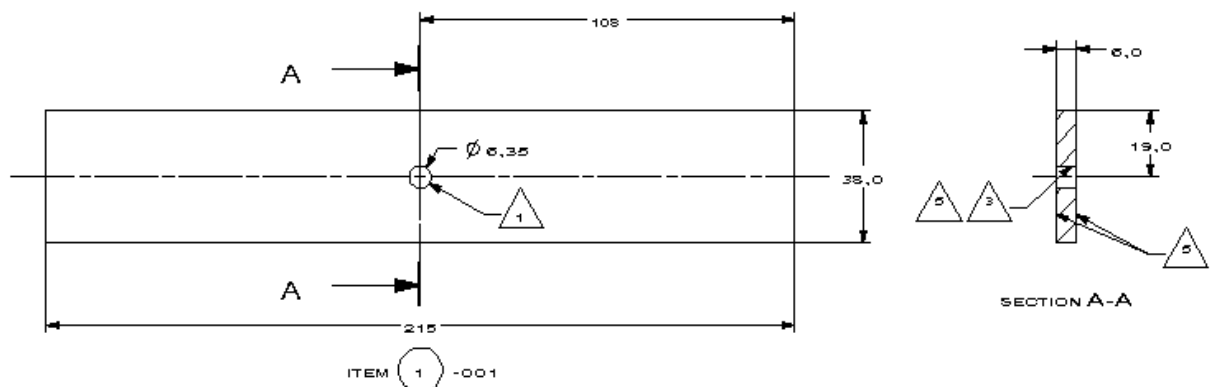


**Figure 25: Fatigue Test Coupon to Determine the Shape-Factor Parameter ( $\beta$ ) for 7050-T74 Structures.**

All the coupons were tested to failure under a constant amplitude spectrum having a maximum remote stress of 14.62 Ksi, at  $R = -1$ . (The net-stress was  $\pm 17.53$  Ksi.)

All ten coupons were equipped with four crack wires near the edges of the hole (both sides of the coupon) in order to detect crack growth.

The shape-factor parameters ( $\beta$ ) were determined by performing a Weibull analysis of the crack-detection lives and failure lives, using the SuperSmith Software (Reference Y).

Figure 26 shows the Weibull plot for the earliest crack-detection and failure of the ten coupons. The data shows very good correlation with the Weibull distribution for both crack-detection and failure lives. The characteristic lives ( $\eta$ ) were found to be 62,100 and 80,800 cycles respectively, while the Weibull shape-factors ( $\beta$ ) were found to be 7.78 and 9.51 respectively. These shape-factors are significantly *higher* than the typical Weibayes shape-factor of 4.0 that is often quoted in the literature. This means *carefully manufactured* nearly-identical specimens may have fatigue life scatter considerably lower than what was previously assumed. Additional testing is needed to confirm these results.

Figure 27 shows the "likelihood contours" for  $\eta$  and  $\beta$  for the earliest-detection and failure of the 10 coupons, for several confidence levels. For a 95% confidence level, the lowest values of the shape-factor ( $\beta$ ) are 5.1 and 6.1 respectively.

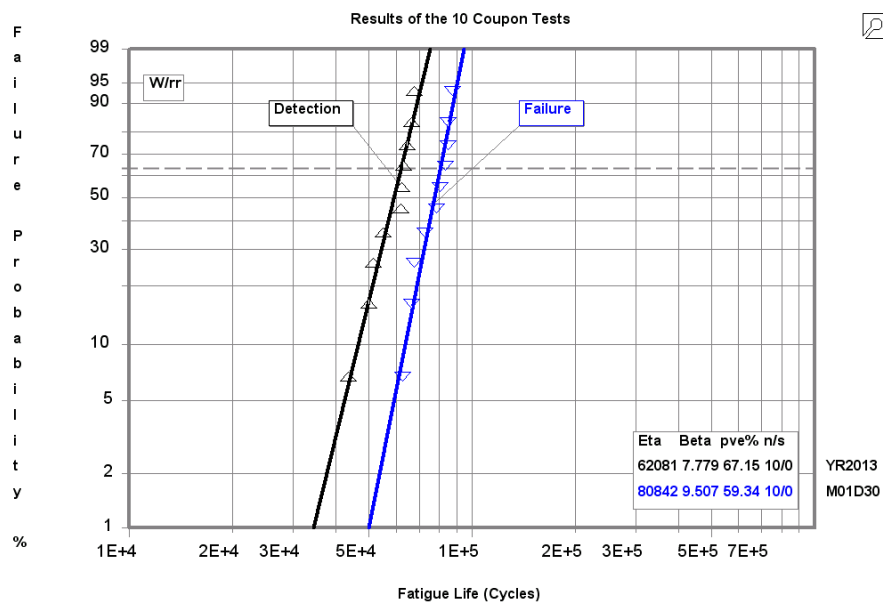


Figure 26: Weibull Plot of the Results of the Ten Coupon Tests

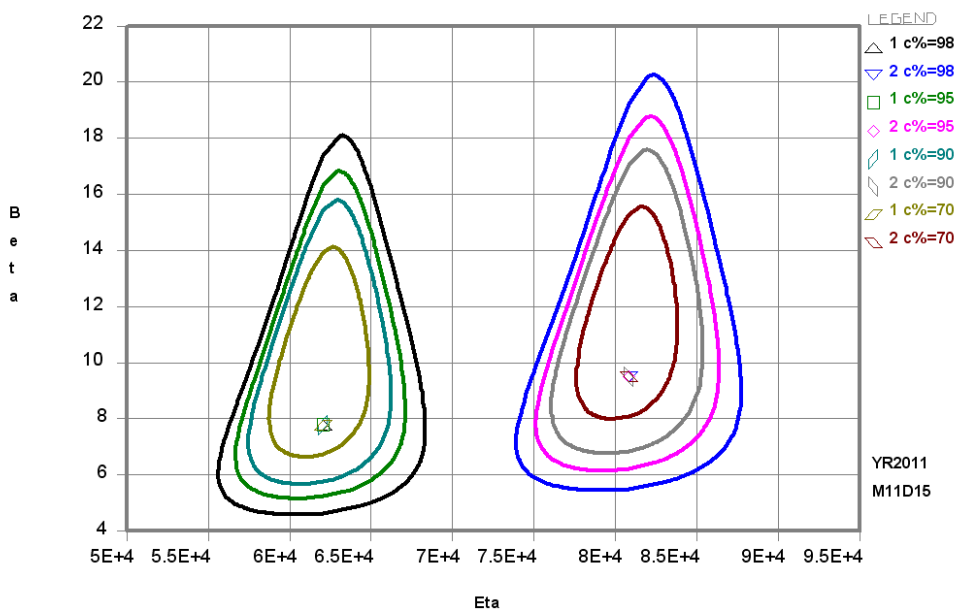


Figure 27: Likelihood Contours of Characteristic Life ( $\eta$ ) and Weibull Shape-Factor ( $\beta$ ). (Left curve is for crack detection; Right curve is for failure; 70%, 90%, 95% and 98% Confidence Contours are shown)

## 5. MISCELLANEOUS

### 5.1 TaxiBot - A New Concept for Towing Airplanes with Engines Stopped (A. Perry, IAI)

This activity is a continuation of a study that was presented in the 2011 Israel national review [1].

Since the start of the widespread use of towbarless towing, there have been many attempts to tow aircraft directly from the gate to the takeoff runway (dispatch /operational towing) with the engines stopped, in order to save fuel and reduce noxious gases and noise pollution. In the past, these proposals have all been dismissed by the airframe manufacturers due to the expected reduction of the fatigue life of the nose landing gear, due to the many towing load cycles that will be applied during dispatch towing.

Nevertheless, the dispatch towing concept has many advantages. A study has shown that an annual savings of \$7.3 billion of fuel expenses and 23 million tons of CO2 emission can be realized, if all wide-body and narrow-body aircraft are towed to their takeoff points. *(A large wide-body aircraft burns about 355 gallons of fuel for every 17 minutes of taxi-out time needed to reach its takeoff point)*

IAI, together with Airbus and other subcontractors, has developed a semi-robotic towbarless towing vehicle called TaxiBot (Taxiing Robot). Under this concept, the pilot of the aircraft remains in full command during the entire towing process, in contrast with the regular dispatch towing where the driver is in control. In order to slow down and /or stop, the pilot will apply the aircraft brakes (the Main Landing Gears) as needed, as opposed to regular dispatch towing where the tractor was stopping the convoy. By slowing / stopping the convoy by the airplane, the magnitude of the load applied on the Nose Gear is reduced significantly, by the airplane-to-tug mass ratio (10 for wide-body airplanes). The airplane engines will be started-up only shortly before takeoff.

This concept has been proved during a TaxiBot Demonstrator testing, see Figure 28. Test measurements have confirmed that TaxiBot towing will not result in any reduction of the Nose Landing Gear fatigue life.



**Figure 28: Airbus A340-600 and Boeing B747-400 towed by TaxiBot**

The next step was to build a Prototype to tow narrow-body (NB) airplanes, to integrate, test and certify. The French company TLD, the biggest GSE manufacturer, produced the TaxiBot NB prototype vehicle which is tested these days in Chateauroux airfield in France.

The program acquired a grounded A320-200 airplane and instrumented it to serve as realistic test-bed, see Figure 29. TaxiBot NB is in the process of final development tests, certification and serial production is scheduled to be completed by end of 2013.

The TaxiBot wide-body (WB) prototype is in its final design stage, vehicle will be operational Q1 2014, final testing and certification is scheduled by Q3 and serial production by end of 2014.

Lufthansa supported the program from day one, followed the development over the years, donated the demonstrator vehicle that was modified with all TaxiBot features (Figure 28), provided precious data, information and operational concepts for taxiing. Lufthansa will be the first to introduce TaxiBot in its fleet and towards this end, it will conduct a Beta Site beginning Q3 2013 operating three NB TaxiBots for a trial period of six months towing actual airplanes with passengers at Frankfurt Airport in Germany.



**Figure 29: TaxiBot NB prototype towing the Airbus A320-200**

Summary: TaxiBot, a green taxiing solution now!

- The TaxiBot program is an excellent encounter between economical and environmental interests
- It is compatible with aircraft having 100 seats or more (Boeing or Airbus)
- Provides an immediate *green* solution
- Does not affect the fatigue life of the nose landing gear or its attachments
- Introduces revolution to a conservative industry
- Incorporates a safety driver
- Maintains the pilot's responsibility (while being transparent)
- Works closely with airlines and airports
- Minor or no adaptations are needed for system implementation (airport or airplane)
- No additional weight added to any airplane
- The only solution to reduce taxiing fuel consumption as early as 2013
- A transparent system to pilot operation as per pilot feedback from tests
- A solution that will work for narrow-body and also wide-body aircraft
- The only solution that will remain available for years on current aircraft fleets

## 5.2 Progress at the Dreszer Fracture Mechanics Laboratory (L. Banks-Sills, TAU)

During the last two years, characterization of the behavior of delaminations between layers of fiber reinforced, laminate composite material has been continuing. A graduate student completed her M.Sc. thesis on calculating stress intensity factors for a delamination between a unidirectional composite and a woven composite [18]. The asymptotic stress and displacement fields were derived. As an outcome of this study, presentations were made at the International Society for the Interaction of Mechanics and Mathematics, STAMM XVIII Symposium in Haifa, Israel [19] and at the International Congress of Theoretical and Applied Mechanics (ICTAM) in Beijing, China [20]. These studies are continuing with tests to be carried out on Brazilian disk specimens containing composite material with a delamination along this interface.

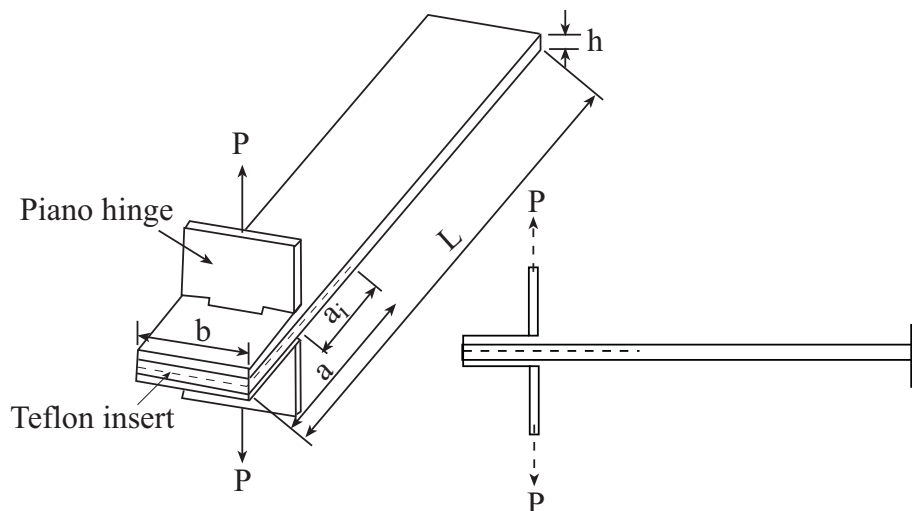
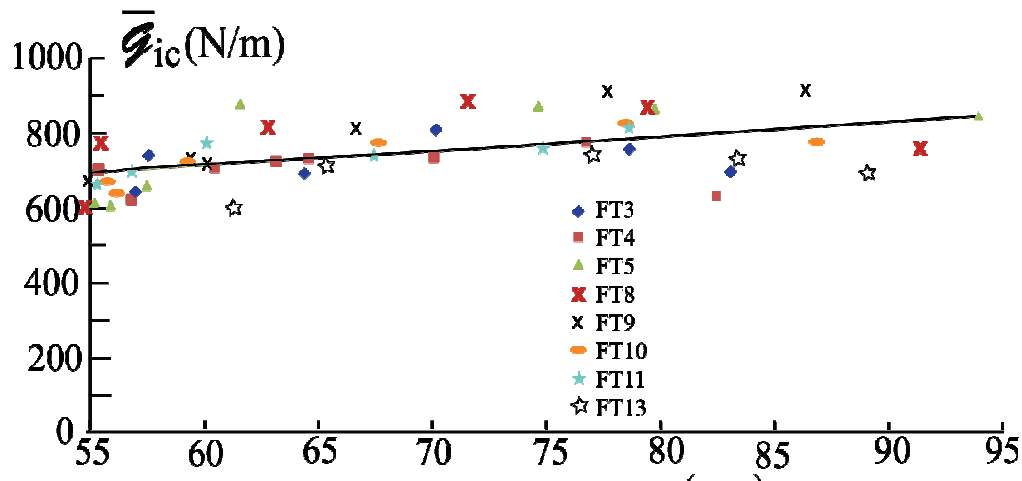


**Figure 30: Double cantilever beam woven composite specimen.**

Another investigation which is being carried out is that of determining the nearly mode I interface fracture toughness  $G_{ic}$  in a multi-directional woven composite. Note that the subscript  $i$  represents interface. A double cantilever beam (DCB) specimen was used for the tests as shown in Fig. 30. The specimen was comprised of 15 layers alternating between a  $0^\circ/90^\circ$  weave and a  $+45^\circ/-45^\circ$  weave. Analysis of the tests showed a slowly rising  $G_R$ -curve (see Fig. 31). Different parts of this work were presented at the Third Broberg Symposium, Lund, Sweden [21], the Society of Experimental Mechanics, Costa Mesa, California [22], the European Conference of Fracture (ECF19), Kazan, Russia [23] and a paper was published in the Proceedings of the 51<sup>st</sup> Israel Annual



Figure



Figure 32: Four-point bend specimen with copper electrodes attached.

Studies on the cracking of piezoelectric materials have continued. There are four intensity factors for cracks in piezoelectric materials: the usual stress intensity factors for the three modes of deformation  $K_I$ ,  $K_{II}$  and  $K_{III}$  and a fourth intensity factor  $K_{IV}$  related to the electric flux density vector  $D_I$ . A paper was published last year on this subject [25]. This study focused on the behavior of a crack in piezoelectric material in which the crack is parallel to the poling direction. Tests were carried out on four-point bend specimens made of PZT-5H (see Fig. 32).

Cracks were introduced parallel to the poling direction. With an electric field induced perpendicular to the cracks, the load was increased until failure occurred. Using the load at fracture, the level of the electric field and the critical crack length, finite element analyses were carried out to determine the intensity factors. These included  $K_I$ ,  $K_{IV}$  and a small  $K_{II}$  component. The latter occurred because of the small asymmetry of the crack.

The material within the crack (air) was modeled to be a dielectric material. A fracture criterion was implemented in which the test results show small scatter about the failure curve. These tests were carried out in order to improve on the scatter obtained from a previous set of tests presented in Motola et al. [26]. The scatter from those results was explored and seen to be a result of the poorly induced notches.

Finally in [27], crack tip conditions in SUS 304 austenitic stainless steel were studied using a constitutive model in which the martensitic phase transformation is an integral part. The phase transformation occurring in the crack tip region gives rise to fracture toughening of the material whereby the resistance against crack initiation, as well as the macroscopic material response, is strongly altered by the presence of a martensitic phase. The constitutive model employed permitted study of the transformation zones under different isothermal conditions. Local crack tip conditions and related plastic deformation was confirmed to depend strongly on the varying extent of the martensitic phase transformation at different temperatures. The shape and size of the plastic and transformation zones in the neighborhood of the crack tip were obtained from numerical simulations, as well as derived analytically.

### 5.3 Low-Cycle Fatigue of Light Materials for Aerospace Applications (Y. Unigovski, A. Grinberg, E. M. Gutman, BGU)

In spite of a relatively large amount of data on flexural fatigue of aluminum alloys and carbon-epoxy laminates, their fatigue behavior is not studied in-depth. Low-cycle fatigue (LCF) of 1.6-mm-thick 6061-T6 Al alloy plated with nickel, gold and silver as well as thermally-cycled carbon-epoxy laminate is studied in this paper at constant strain in a purely bending mode. The dynamics of the crack propagation was investigated in details using microscopic methods (Fig. 33). The tensile and fatigue properties of the alloy coated with multi-layered deposits depend, first of all, on the thickness of the inner electroless nickel layer that drastically decreases the ductility of the system. Electroplating by the second ductile Ni layer increases the lifetime of the alloy in comparison with that coated only by the electroless Ni layer.

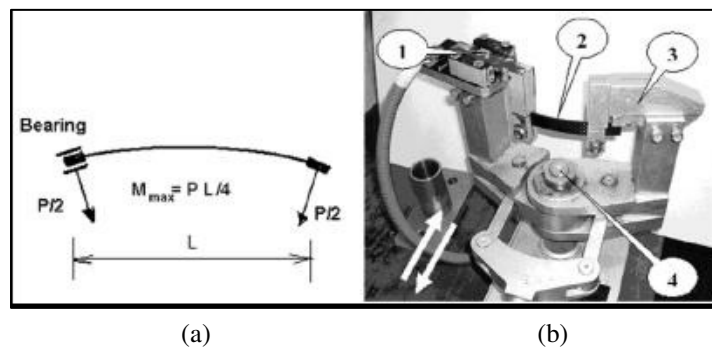


**Fig. 33. Scheme (a) and view (b) of the sample grip of IP-2 pure bending machine.**

**1 – first twist grip with a possibility for reciprocal motion, 2 – sample, 3 – second twist grip, 4 – pivot pin.**

Carbon-epoxy 3-mm-thick composite demonstrated a catastrophic shortening of the fatigue life  $N$  already at very small increase in the plastic strain amplitude. For example, increasing  $\Delta\varepsilon_p$  from 0.002 to 0.003 in a reversible mode causes a decrease in lifetime by an order of magnitude (from  $10^4$  to  $10^3$  cycles). Thermal cycling of the composite at maximum and minimum operating temperatures of  $180^\circ\text{C}$  and  $-195.8^\circ\text{C}$ , respectively, shortens the fatigue life of samples at relatively small plastic deformation and the number of cycles  $N$  exceeding 20,000. An inversion point in a  $\log\Delta\varepsilon_p - \log N$  plot was found at such  $N$  value, namely, at  $N \leq 20,000$  the fatigue life of thermally-cycled laminates was slightly longer than that of the reference one. This behavior of thermally-cycled laminate at relatively high plastic strain amplitudes, probably, is due to the stress distribution between small cracks, which retards the fatigue failure and prevents fast propagation of the main crack. Photos taken by SEM demonstrating the degradation in fatigue and crack growth properties are presented in Fig. 34.

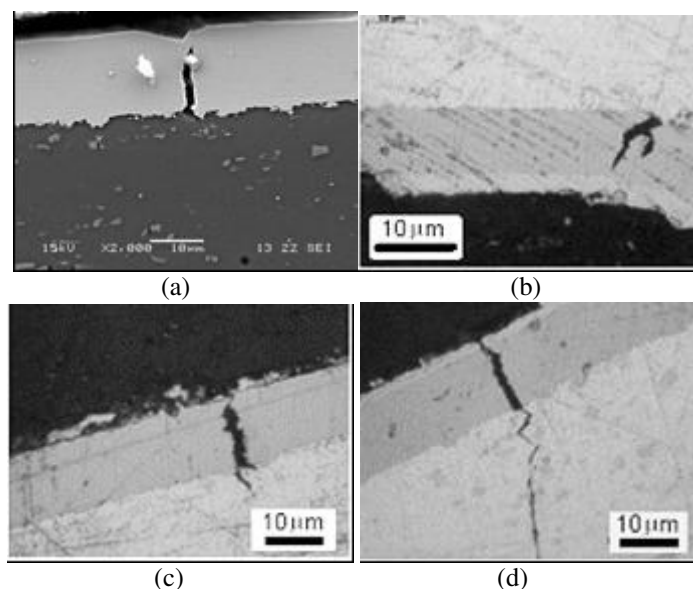


**Fig. 34. SEM (a) and optical (b, c, d) micrographs of cracks in samples of set 4 originated at the interface between electroless nickel layer and Al substrate at  $\Delta\varepsilon_{pl}$ : 0.010 (a) and 0.005 (b, c, d). Number of cycles: 1 (a); 1253 or  $0.2N_f$  (b), 2505 or  $0.4N_f$  (c) and 5010 or  $0.8N_f$  (d).**

The results of this study will be presented as a poster in the 27<sup>th</sup> ICAF symposium, 2013 [28].

#### 5.4 A Failure Initiation Criterion for 3-D Elastic Brittle Structures (B. Ben-Ami, Z. Yosibash, BGU)

There is no validated failure criterion in the vicinity of V-notches and cracks known to the authors for failure initiation in a 3-D brittle elastic body. Most available failure criteria are based on 2-D assumptions. These assumptions do not enable a formulation of a failure initiation criterion under general loading conditions which involves out of plane shear (mode III). We aim at formulating a failure criterion in brittle isotropic materials containing a sharp V-notch, employing analytical, numerical and experimental aspects.

Several tests were conducted for the determination of the failure criterion. The specimens used for the experiments were bars containing a V-notch inclined to its facet ( $\beta$  is the inclination angle in relation to the normal to the specimen surface), under four point bending (4PB) load (see Fig.35 for specimen geometry).

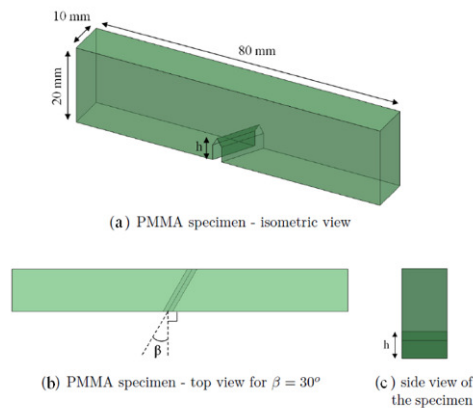


**Fig. 35. PMMA Specimen Geometry and Dimensions**

Fracture tests were performed on such bar specimens using a Zwick testing machine 1445, with nominal load capability of 10kN. A Vishay system 7000 was used to record the load cell output and displacements at a chosen point, by means of displacement sensors. The Vishay 7000 system was connected to the Zwick and records the load cell output via an amplifier (precision of  $\pm 0.5\%$  [N]). In addition, an external linear displacement sensor was connected to the Vishay 7000 system (precision of  $\pm 0.1\%$  [mm]). The tip of the sensor is round so that it approximately samples the displacement at a point. This sensor was always located at the center of the specimen upper face (see Fig. 36).

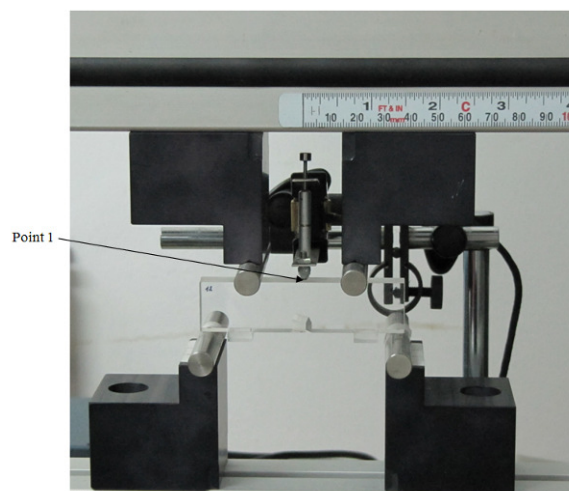


**Fig. 36. 4PB Test Configuration**

A general trend was observed from the experiments in which the number of fracture origins along the notch front decreases as the inclination angle  $\beta$  increases. The new criterion should, therefore, be able to describe a point-wise, segmented, or continuous fracture.

Elastic solution of the near crack tip behavior was developed. Numerical analysis was conducted to obtain The generalized edge stress intensity functions  $A_i(z)$  along the notch edge, so that the stress and displacement fields in the vicinity of the notch edge will be determined.

Finally, by exploiting the test results and the analytical and numerical analyses conducted, three-dimensional failure criterion for V-notched specimens was established. The failure criterion was derived as a generalization of the two dimension failure criterion for V-notched specimens, that was introduced by Leguillon and Yosibash. The formulation of the new 3-D failure criterion and its validation by the presented experimental observations will be reported in a future publication.

This study will be presented as a poster in the 27<sup>th</sup> ICAF symposium, 2013 [29].

### 5.5 Edge Stress-Intensity Functions for Circular Cracks in a 3-D Elastic Domain (S. Shannon, Z. Yosibash, BGU)

The elastic solution in 2-D domains in non-smooth domains like polygons, is known to be described in terms of special singular functions depending on the geometry and the differential operators on one hand, and of unknown coefficients depending on the given right hand side and boundary conditions, on the other hand. In three-dimensional domains, as a polyhedral. Explicit representation of the solution is given as a series characterized by: eigen-values  $\alpha_i$ , their corresponding eigen-functions and shadow-functions  $\Phi_{il}(\varphi)$ , and their corresponding edge stress intensity functions  $A_i(z)$ , which are functions along the edge. In this investigation, the authors concentrate on circular edges such as “penny-shaped crack”, and derive explicitly singular series expansion in the vicinity of such an edge for the elasticity system. A cross section of the concerned problem is given in Figure 37. The paper provides explicitly the asymptotic solution for the elasticity system in the simplified case of the penny-shaped crack under axisymmetric and non-axisymmetric boundary conditions.

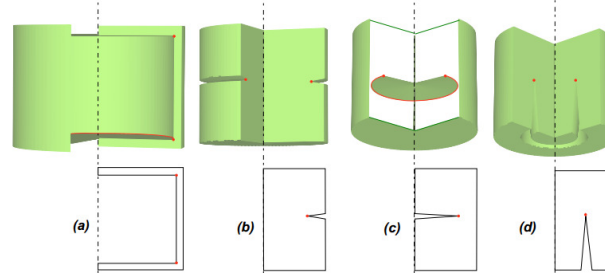


**Figure 37. Different types of singular circular. The domain in (c) includes the renowned "penny-shaped" crack.**

After deriving the explicit asymptotic elastic solution, the stress intensity functions along the circular singular edges are obtained numerically by means of three dimensional J-integral and the Quasi-Dual Function Method (QDFM). The full length paper demonstrates that the edge stress intensity functions are easily obtained without the need of a refined mesh in the vicinity of the circular crack front and they are obtained as functions along the circular edge.

This study will be presented as a poster in the 27<sup>th</sup> ICAF symposium, 2013 [30].

### 5.6 Progress at BGU Computational Mechanics Laboratory (Z. Yosibash, BGU)

In 2012, a book by Z. Yosibash on topics with interest of ICAF audience was published by Springer [31]. This introductory and self-contained book gathers as much explicit mathematical results on the linear-elastic and heat-conduction solutions in the neighborhood of singular points in two-dimensional domains, and singular edges and vertices in three-dimensional domains. These are presented in an engineering terminology for practical usage. The book provides the mathematical formulations from an engineering viewpoint and present high-order finite-element methods for the computation of singular solutions in isotropic and anisotropic materials, and multi-material interfaces. The proper interpretation of the results in engineering practice is advocated, so that the computed data can be correlated to experimental observations.

Most of it (the first nine Chapters) addresses two-dimensional domains, where only singular points exist. The thermo-elastic system and the feasibility of using the eigenpairs and generalized stress-intensity factors for

predicting failure initiation in brittle material on a daily basis engineering practice is addressed. Several failure laws for two-dimensional domains with V-notches are presented and their validity is examined by comparison to experimental observations. A sufficient simple and reliable condition for predicting failure initiation (crack formation) in micron level electronic devices, involving singular points, is still a topic of active research and interest, and is addressed herein.

Explicit singular solutions in the vicinity of vertices and edges in three-dimensional domains are provided in the remaining five Chapters. New methods for the computation of generalized edge flux/stress intensity functions along singular edges are presented and demonstrated by several example problems from the field of fracture mechanics; including anisotropic domains and bimaterial interfaces. Circular edges are also presented and we conclude with some remarks on open questions.

Elasticity problems having curved edges in three-dimensional (3-D) domains have been also investigated recently by Z. Yosibash and collaborators [32, 33]. In [32], the asymptotic solutions to the Laplace equation and the elasticity system in the vicinity of a circular singular edge in a three-dimensional domain were derived, and are provided in an explicit form. These asymptotic solutions are represented by a family of eigen-functions with their shadows, and the associated generalized edge flux/stress intensity functions (GEFIFs/GESIFs), which are functions along the circular edge. Explicit formulas for a penny-shaped crack for an axisymmetric case as well as a case in which the loading is nonaxisymmetric were provided.

In [33], the explicit solution representation derived in [32] was employed to extend the quasidual function method (QDFM) for extracting the GEFIFs along circular singular edges in the cases of axisymmetric and non-axisymmetric data. This accurate and efficient method provides a functional approximation of the GEFIFs along the circular edge whose order is adaptively increased to approximate the exact GEFIFs. It is implemented as a post-solution operation in conjunction with the p-version of the finite element method. The mathematical analysis of the QDFM was provided, followed by numerical investigations, demonstrating the efficiency, robustness and high accuracy of the proposed quasi-dual function method. The mathematical machinery developed in the framework of the Laplace operator is important to realize its possible extension for the elasticity system.

### **5.7 Time Reversal as a Computational Tool for Crack Identification (E. Amitt & D. Givoli, Technion, and E. Turkel, TAU)**

In this paper, a combined physical-computational technique is discussed for crack identification, as a tool for Non-Destructive Testing (NDT) of structures. This technique is based on the Time Reversal (TR) approach. First, the basic idea underlying the crack identification method adopted here is described. Then a number of numerical experiments to identify cracks locations via TR are presented.

The system's cracks detection capability is tested for various sizes of cracks, different amounts of available information (different measurement points and measurement times), and various crack orientations. These tests show that the system is successful in most cases in detecting the original locations of the cracks for various sizes and for various amounts of available information. Since in reality no experiments are done in an ideal way, and there is always measurement noise present, the effect of measurement noise on the system is studied.

These experiments lead to the conclusion that the tolerated noise level that maintains the quality of zero-noise refocusing strongly depends on the amount of given spatial and temporal measurement information. Based on all these results, it can be determined that the TR method can be used as an excellent computational tool which supports NDT for structures. It can yield accurate locations (and possibly other parameters) for cracks of different sizes and directions, even under conditions far from ideal.

An example of a successful refocusing is shown in Figure 38.

Fig. 38 (a) shows the original location of the source and Fig. 38 (b) shows the location that was obtained from the TR computation.

The results of this study will be presented at the 27<sup>th</sup> ICAF Symposium (2013) [34].

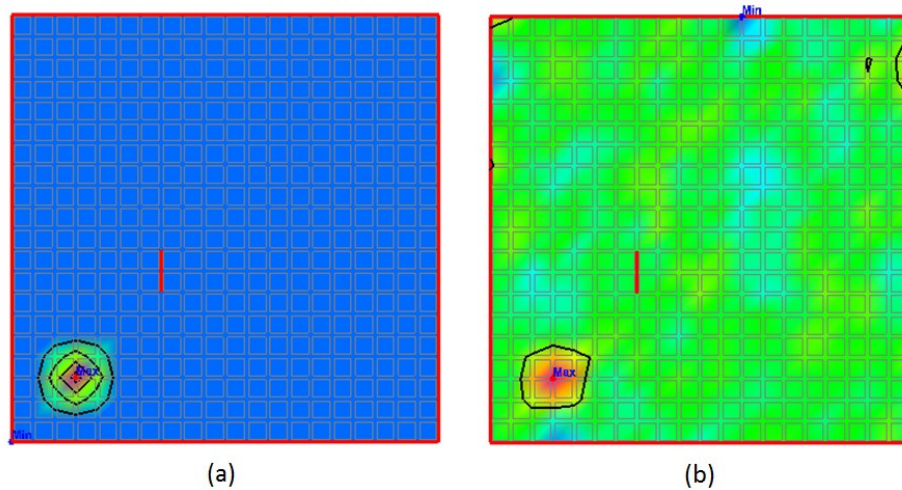


**Figure 38: Example of a successful refocusing using TR. (a) The original condition function; (b) The results obtained from TR**

### 5.8 The Investigation of Fatigue Models (E. Rejovitzky, and E. Altus, Technion)

A stochastic two-parameter Micromechanical Fatigue Model (MFM), which considers morphological aspects of microcrack coalescence and arrest, has been proposed. The material is modeled as an ensemble of elements with a stochastic failure strain distribution. By using set theory tools, equilibrium and material strength partitioning, an analytical fatigue life relation is obtained. The cycle-by-cycle damage evolution is transformed into a continuous form, leading to a non-linear separable differential equation. An exact solution of this equation yields the familiar stress-life power-law ( $r = AN^b$ ) and endurance limit. These are directly related to two characteristic micromechanical parameters of material heterogeneity: the strength distribution shape factor of the ensemble and the microcrack arrest probability. The model proposes a new generic relation between the damage evolution function and the S–N power-law, which is validated by recent experiments for three different steels studied elsewhere. The damage evolution morphology includes the full microcrack size distribution. Good prediction capabilities are obtained for high-to-low two-level fatigue loading based on single-level data only [35].

In another study, fatigue life tests under varying stress levels have revealed deviations from the linear Palmgren-Miner (PM) rule. The non-commutative damage accumulation has been demonstrated in two-level fatigue tests: longer life under low-to-high (L-H) loading order and shorter life for H-L loading order. Tests under random loading were also far from the PM predictions. A consistent Fiber Bundle Model (FBM) was presented which follows microcrack initiation, growth and coalescence. Using a commutative microcrack initiation law, we improve our earlier work, and obtain the damage evolution and Basquin's power law analytically. It is shown that the macro non-commutative behavior is dominated by material heterogeneity, which controls the microcrack initiation morphology. Fatigue life under two-level loading and under random loading is found analytically and relations between micro-parameters and macro stress-life results are revealed [36].

A third study focuses on an analytical investigation of the common characteristics of fatigue models based on a Single Damage Variable (SDV). The general SDV constitutive equation is used to extract several fundamental properties. It is shown that damage evolutions under constant loads are sufficient for predicting fatigue life under any load history. Two-level fatigue envelopes constitute an indirect measure of the damage evolution and form an alternative basis for life prediction. In addition, High to Low (H-L) and Low to High (L-H) failure envelopes are anti-symmetrical with respect to one another. A new integral formula for life prediction under random loads is developed and applied on two well known SDV models, resulting in analytical predictions. The Palmgren-Miner rule is found to yield an upper bound for random fatigue life predictions of all SDV models [37].

## 6. REFERENCES

1. Brot, A., "Review of Aeronautical Fatigue Investigations in Israel, April 2009 – March 2011", *Minutes of the 32<sup>nd</sup> ICAF Conference*, Montreal, Canada, 2011.
2. Brot, A., and Matias, C., "An Evaluation of Several Retardation Models for Crack Growth Prediction under Spectrum Loading", *USAF Aircraft Structural Integrity Program Conference*, Savannah, GA, December 2002.
3. Matias, C., and Katsav, E. "Evaluation of the Strip-Yield Retardation Model for Predictions of Fatigue Crack Growth under Typical Aircraft Loading Spectra", *Proceedings of the 27<sup>th</sup> ICAF Symposium*, Jerusalem, Israel, 2013.
4. Brot, A., "Developing Strategies to Combat Threats against the Structural Integrity of Aircraft", *Proceedings of the 52<sup>nd</sup> Israel Annual Conference on Aerospace Sciences*, 2012.
5. Brot, A., "Optimizing the Inspection Intervals for Aircraft Structures Prone to Multi-Site Damage", *Proceedings of the 53<sup>rd</sup> Israel Annual Conference on Aerospace Sciences*, 2013.
6. Freed, Y., Dolev, O., et al, "Failure Investigation of Fatigue Cracks Initiated at Business Jet Vertical Tail Drag Angles", *Proceedings of the 53<sup>rd</sup> Israel Annual Conference on Aerospace Sciences*, 2013.
7. Freed, Y., "G280 Executive Jet – Full Scale Fatigue Testing", *Proceedings of the 52<sup>nd</sup> Israel Annual Conference on Aerospace Sciences*, 2012.
8. Sadananda K., Vasudevan A. K., "Short crack growth behavior", *Fatigue and Fracture Mechanics: 27th Volume*, ASTM-STP 1296, ASTM PA, 1997:301-316.
9. Sadananda K., Vasudevan A. K., "Analysis of small crack growth behavior using unified approach" *Small Fatigue Cracks: Mechanics, Mechanisms and Application*, Ritchie R.O. and Murakami Y., (eds.), Elsevier, 1999:73-83.
10. Sadananda K., Vasudevan A. K., "Short crack growth and internal stresses", *Int. J. of Fatigue* 1997:19(93):S99-S108.
11. Maymon, G., "Several Models for Crack Propagation", *Proceedings of the 53<sup>rd</sup> Israel Annual Conference on Aerospace Sciences*, 2013.
12. Minz and L., Gur, I., "Tolerance-Based Regime Recognition Algorithm Methodology (RRA) for AH64", *Proceedings of the 52<sup>nd</sup> Israel Annual Conference on Aerospace Sciences*, 2012.
13. Kedem, S., et al, "Emergency Repair Design for a Refueling Boom". *Proceedings of the 27<sup>th</sup> ICAF Symposium*, Jerusalem, Israel, 2013.
14. Nakada, M. and Miyano., L., "Accelerated Testing for Long-Term Fatigue Strength of various FRP Laminates for Marine use", *Composites Science and Technology* 69 (2009), p. 805-813.
15. Freed, Y., Pantou, R., Buimovich, Y. and Rzepka, S., "Accelerated Testing Methodology for the Predictions of Long Term Strength and Durability of Composite Materials in Marine Environment", *Proceedings of the 27<sup>th</sup> ICAF Symposium*, Jerusalem, Israel, 2013.
16. Freed, Y., and Rzepka, S., "An Implementation of an Accelerated Testing Methodology to Obtain Static, Creep and Fatigue Master Curves of T300/913 Unidirectional Composite Material", *Proceedings of the 26<sup>th</sup> ICAF Symposium*, 2011.

17. Kressel, I., Tur, M., et al, "Fiber-Optic Based Technology for UAV Structural Health Monitoring", *Proceedings of the 27<sup>th</sup> ICAF Symposium*, Jerusalem, Israel, 2013.
18. Gohfeld, M., "Calculation of Stress Intensity Factors for a Delamination Between Two Composite Materials: Upper Material – Unidirectional Composite, 90°, Lower Material – Balanced Plain Weave, (0°/90°)", M.Sc., Tel Aviv University, 2013.
19. Banks-Sills, L., Gohfeld, M., and Eliasi, R., "Delaminations in Multi-directional and Woven Composites", STAMM, Haifa, Israel, 2012.
20. Banks-Sills, L., Gohfeld, M., and Eliasi, R., "Delamination between a Unidirectional and Woven Composite", *International Congress of Theoretical and Applied Mechanics*, Beijing, China, 2012.
21. Banks-Sills, L., Ishbir, C., et al, "Crack Resistance Curves Obtained from DCB Specimens Composed of Woven Composites", *Third Broberg Symposium*, Lund, Sweden, 2011.
22. Banks-Sills, L., Ishbir, C., et al, "Delamination Toughness Tests of DCB Specimens Composed of Woven Composites", *Society of Experimental Mechanics*, Costa Mesa, California, 2012.
23. Banks-Sills, L., Ishbir, C., et al, "Testing of DCB Specimens Composed of Woven Composites", *European Conference of Fracture (ECF19)*, Kazan, Russia, 2012.
24. Ishbir, C., Banks-Sills, L., et al, "Interface Fracture Behavior of Plain Laminate Woven Composites (the 0°/90° – +45°/-45° Interface)", *Proceedings of the 52<sup>nd</sup> Israel Annual Conference on Aerospace Sciences*, 2012.
25. Banks-Sills, L., Heller, L. and Fourman, V., "A Supplementary Study on Fracture Tests of Piezoelectric Material: Cracks Parallel to the Poling Direction", *International Journal of Fracture*, 175, (2012f) 109–125, DOI 10.1007/s10704-012-9706-2.
26. Motola, Y., Banks-Sills, L. and Fourman, V., "On Fracture Testing of Piezoelectric Ceramics", *International Journal of Fracture*, 159 (2009) 167–190, DOI 10.1007/s10704-009-9392-x.
27. Hallberg, H., Banks-Sills, L. and Ristinmaa, M., "Crack Tip Transformation Zones in Austenitic Stainless Steel ", *Engineering Fracture Mechanics*, 79 (2012) 266–280, DOI:10.1016/j.engfrac\_mech.2011.11.004.
28. Unigovski, Y., Grinberg, A. and Gutman, E. M, "Low-Cycle Fatigue of Light Materials for Aerospace Applications", *Proceedings of the 27th ICAF Symposium*, Jerusalem, Israel, 2013.
29. Ben-Ami, B. and Yosibash., "A Failure Initiation Criterion for 3-D Elastic Brittle Structures", *Proceedings of the 27th ICAF Symposium*, Jerusalem, Israel, 2013.
30. Shannon, S. and Yosibash., "Edge Stress Intensity Functions for Circular Cracks in a 3-D Elastic Domain", *Proceedings of the 27th ICAF Symposium*, Jerusalem, Israel, 2013.
31. Yosibash Z., "Singularities in Elliptic Boundary Value Problems and Elasticity and their Connection with Failure Initiation", *Springer*, ISBN 978-1-4614-1507-7, 2012.
32. Yosibash Z., Shannon S., Dauge M. and Costabel M., "Circular Edge Singularities for the Laplace Equation and the Elasticity System in 3-D Domains", *International Journal of Fracture*, 168, 2011, pp. 31–52.
33. Shannon S., Yosibash Z., Dauge M. and Costabel M., "Extracting Generalized Edge Flux Intensity Functions by the Quasidual Function Method along Circular 3-D Edges", *International Journal of Fracture*, 2012, Submitted.
34. Amitt, E., Givoli, Turkel, E., "Time Reversal as a Computational Tool for Crack Identification", *Proceedings of the 27th ICAF Symposium*, Jerusalem, Israel, 2013.



35. Rejovitzky, E. and Altus, E., "A Micromechanical Fatigue Model with Damage Morphology", *International Journal of Fatigue* 33 (2011) 1235–1243.
36. Rejovitzky, E. and Altus, E., "Non-Commutative Fatigue Damage Evolution by Material Heterogeneity", *International Journal of Fatigue*, Submitted 2011.
37. Rejovitzky, E. and Altus, E., "On Single Damage Variable Models for Fatigue", Internal Technion Report, 2011.